The link transmission model with variable fundamental diagrams and initial conditions

van der Gun, Jeroen; Pel, Adam; van Arem, Bart

DOI
10.1080/21680566.2018.1517060

Publication date
2018

Document Version
Final published version

Published in
Transportmetrica B: Transport Dynamics

TRANSPORTMETRICA B: TRANSPORT DYNAMICS
https://doi.org/10.1080/21680566.2018.1517060

Taylor & Francis
Taylor & Francis Group

The link transmission model with variable fundamental diagrams and initial conditions

Jeroen P. T. van der Gun, Adam J. Pel and Bart van Arem

Department of Transport & Planning, Delft University of Technology, Delft, Netherlands

ABSTRACT

The link transmission model is a macroscopic network traffic flow simulation tool based on Lighthill–Whitham–Richards theory. While its efficiency and accuracy are superior to the well-known cell transmission model, applications of its current numerical formulations are limited by the inability to apply changes to the fundamental diagrams of links within a simulation and the need to start the simulation with an empty network. We resolve both limitations by developing a methodology for initialising the discrete-time link model with a non-empty initial condition and for computing within-link densities during the simulation, which can then serve as an initial condition for continued simulation with a new fundamental diagram. Since the computation of within-link densities is algebraic, no new numerical errors are introduced. Optional support for multiple commodities, subcritical delays and platoon dispersion, are retained. The resulting model is demonstrated on a motorway corridor network with variable speed limits and dynamic lane management.

ARTICLE HISTORY
Received 2 November 2017
Accepted 24 August 2018

KEYWORDS
Link transmission model; first-order model; Smulders fundamental diagram; traffic control; environmental conditions

1. Introduction

Lighthill and Whitham (1955) and Richards (1956) were the first to model traffic flow using a differential equation combining conservation of vehicles with an equilibrium flow-density relationship referred to as the fundamental diagram (FD). The traditional cell-based numerical solution scheme to this Lighthill–Whitham–Richards (LWR) theory is known as the cell transmission model (CTM) (Daganzo 1994) and can simulate the propagation of traffic in a network of links and nodes using macroscopic variables (Daganzo 1995). While this solution scheme with links discretised into small homogeneous cells is intuitive, it has turned out to be neither the most efficient in terms of computation time nor the most accurate in terms of numerical error. Based on Newell's (1993) recipe using the cumulative numbers of vehicles as the main variable, Yperman, Logghe, and Immers (2005) and Gentile and Papola (2009a, 2009b) developed the link transmission model (LTM). This alternative numerical solution scheme for solving traffic propagation in a network does not discretise links into small cells, improving the efficiency and accuracy compared to the CTM and variants (Yperman, Logghe, and Immers 2005; Yperman 2007, 46–49).

Since then, the LTM has accumulated improvements and extensions. Yperman et al. (2006) developed a multi-commodity version keeping track of heterogeneous traffic composition, to which Yperman (2007) added support for general nodes with multiple incoming and outgoing links. Gentile (2010) added general nodes to his formulation as well. These and other general node models have

CONTACT Jeroen P. T. van der Gun j.p.t.vandergun@tudelft.nl Department of Transport & Planning, Delft University of Technology, P.O. Box 5048, 2600 Delft GA, Netherlands

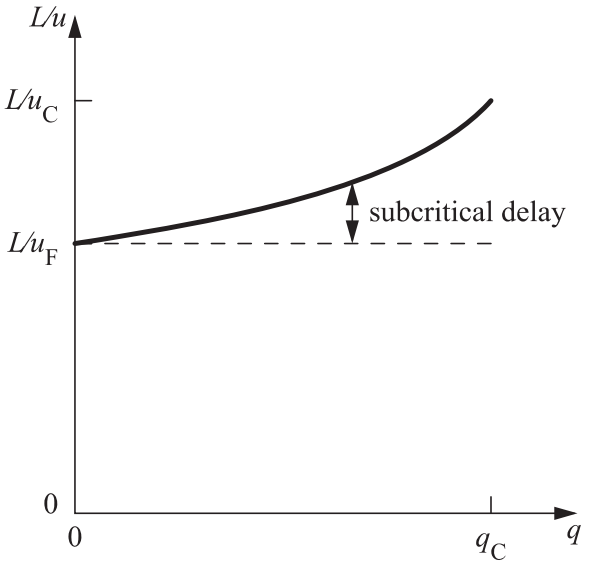

Figure 1. Link travel time L/u in stationary homogenous free-flow conditions as a function of flow q.

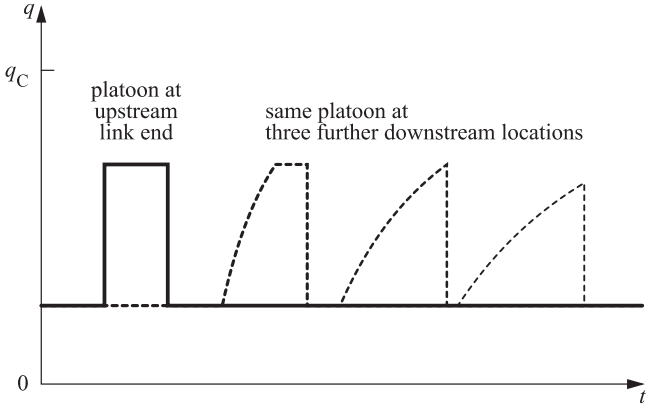

Figure 2. Flow q versus time t at four locations showing platoon dispersion.

further been improved to satisfy the criteria for traffic flow at junctions formulated by Lebacque and Khoshyaran (2005) and Tampère et al. (2011). This resulted in a family of node models described by Smits et al. (2015), and possibilities to simulate signalised junctions (Tampère et al. 2011) and ramp metering (Hajiahmadi et al. 2013).

Furthermore, while the formulations by Yperman, Logghe, and Immers (2005, 2006) were limited to triangular FDs on links, Yperman (2007) proposed piecewise-linear FDs as well, and Gentile and Papola (2009a, 2009b) and Gentile (2010) proposed strictly concave FDs. Such FDs introduce subcritical delays, i.e. demand-dependent increases in link travel time before the capacity of the link is exceeded as illustrated in Figure 1. Due to an initially sharp front of a platoon dispersing into an acceleration fan, they also introduce platoon dispersion as illustrated in Figure 2 (Geroliminis and Skabardonis 2005). Van der Gun, Pel, and Van Arem (2017) improved the numerical accuracy in both proposals and allowed any concave FD. Van der Gun, Pel, and Van Arem (2017) furthermore extended the link and node models to support the capacity drop phenomenon with a mixture of moving jams and standing queues. For

triangular FDs, other link model extensions have been proposed for supporting multiple vehicle types (Smits, Bliemer, and Van Arem 2011) or variable speed limits (Hajiahmadi et al. 2013).

Contrary to the above discrete-time approaches, Raadsen, Bliemer, and Bell (2016a) introduced an event-based continuous-time version of the LTM, to which multi-commodity support and general concave FDs without capacity drop also have been added (Raadsen and Bliemer 2018).

Meanwhile researchers have also been working on creating an iterative variant of the numerical solution scheme (Himpe, Corthout, and Tampère 2016), computing a user-equilibrium traffic assignment (Gentile, Meschini, and Papola 2007; Gentile 2015; Himpe and Tampère 2016; Long, Szeto, and Ding 2017), investigating mathematical properties of the continuous-time network loading (Jin 2015; Han, Piccoli, and Szeto 2016) and user-equilibrium (Han et al. 2015), and utilising the LTM for optimisation purposes (Hajiahmadi 2016; Long et al. 2018; Van de Weg et al. 2016).

1.1. Problem statement

The above literature offers a rich set of features for macroscopically simulating the propagation of traffic in a network over time, also known as dynamic network loading. Nevertheless, except for the triangular-FD variable speed limits model by Hajiahmadi et al. (2013), all of these studies assume that the FDs of all links remain constant during the simulation, which can be problematic for certain applications. Firstly, it precludes time-varying link-based traffic control. Besides variable speed limits, this could also include e.g. temporary lane closures, lane reversal (Wolshon and Lambert 2006), or operation of peak-hour lanes such as hard shoulder running (Sultan, Meekums, and Brown 2008; Geistefeldt 2012; Guerrieri and Mauro 2016). Secondly, it precludes time-varying driving behaviour within a simulation. This may e.g. occur due to changes in precipitation, visibility and road surface conditions (Chung et al. 2006; Rakha et al. 2008; Dixit, Gayah, and Radwan 2012; Kwon, Fu, and Jiang 2013), changes to driver activation levels based on time-of-day (Dixit, Gayah, and Radwan 2012) or evacuation conditions (Yuan, Pel, and Hoogendoorn 2014), or changes to the average vehicle composition over time.

Another drawback of current LTM simulations is the need to start with an empty network. Only Jin (2015) considered more general initial conditions for triangular FDs, but did not develop a numerical solution scheme. This missing feature can also be restrictive, particularly for real-time applications. For example, non-empty initial conditions are used for rolling horizon optimisation of traffic control (Papageorgiou et al. 2003).

The solutions to these two limitations are related. To instantaneously change the FD of a link, it suffices to compute the density of traffic at all places within the link, and use those as the initial condition for a subsequent simulation with the new FD (see Figure 3). In the CTM this is trivial, since the state vector of the model consists entirely of the current cell densities. On the contrary, the LTM state vector does not contain within-link densities and spans more than one time instant. The LTM thus needs to be supplemented with two additional procedures: one to compute the within-link densities, and one to employ these as initial conditions. Hence, although the LTM is normally more efficient than the CTM, it will incur some additional computational cost each time within-link densities need to be used. A convenient property of this setup is that one can even use the within-link densities at time t^* to decide whether and how the FD or within-link should change at the same time t^*. This enables real-time corrections to within-link densities or FD parameters (i.e. data fusion) as well as simulations with real-time traffic-responsive control measures.

1.2. Contribution of this paper

The main contribution of this paper is a novel link model for the discrete-time LTM that includes such methodologies for computing within-link densities and applying initial conditions, offering a single, computationally-efficient, LWR-theory-based simulation tool supporting subcritical delays and platoon dispersion, non-empty initial conditions, computation and modification of densities within links and changes to any FD parameters during the simulation.

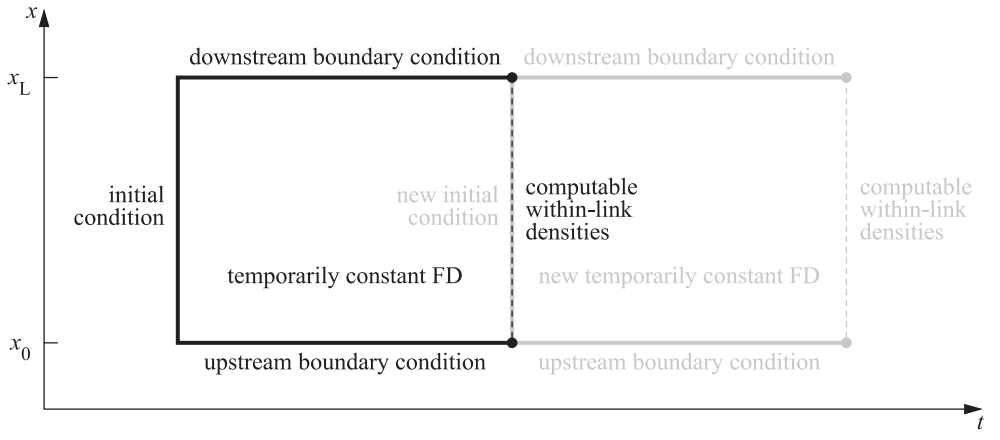

Figure 3. Space–time (x, t) illustration of an FD change for a link from x_0 to x_L.

As shown by Van der Gun, Pel, and Van Arem (2017), it is possible to develop constant-FD discrete-time LTM link models without numerical errors other than those introduced by the time discretisation of node flows. This suggests the possibility of using algebraic descriptions of within-link densities for particular choices of the FD shape, akin to how Raadsen, Bliemer, and Bell (2016a) use boundary flows without numerical errors. This paper will exploit that possibility to avoid introducing any additional numerical errors so that, e.g. changing an FD into an identical FD does not affect the numerical results in any way.

This paper is structured as follows. Section 2 describes the structure of the LTM and explains how our extension is embedded in this structure. Section 3 introduces the main methods needed to construct an LTM link model, relating to the traffic flow theory and the FD. Section 4 applies these methods to formulate our extended LTM link model. A practical demonstration of the extended LTM is provided in the simulation study in Section 5, including comparisons with the unextended LTM and the CTM. This is followed by a discussion of the extended model in Section 6 and our conclusions in Section 7.

2. Structure of the LTM and its extension

The LTM consists of a link model describing traffic flow on homogenous road stretches, and a node model describing traffic flow at discontinuities, including intersections. This section describes the role of both models within the LTM and discusses how they are affected by our extension for variable FDs and initial conditions.

Please note that one can refer to Appendix 1 for a complete overview of all notation that will be introduced in this section and the next two sections.

The link model of the LTM originally consists of two components. The first is the sending flow algorithm that computes the maximum number of vehicles $S(t)$ that can leave the link between now t and some point in the near future $t + \Delta t$, under the assumption that the downstream node does not impose any constraints. Similarly, the second is the receiving flow algorithm that computes the maximum number of vehicles $R(t)$ that can enter the link between now t and some point in the near future $t + \Delta t$, again under the assumption that in this case, the upstream node does not impose any constraints. Both are done by comparing the maximum possible cumulative vehicle number N at the end of the time window $(t, t + \Delta t)$ with the known value of N at the start of the time window:

$$\begin{aligned} S(t) &= N^{\max}(x_L, t + \Delta t_{x_L}) - N(x_L, t) \\ R(t) &= N^{\max}(x_0, t + \Delta t_{x_0}) - N(x_0, t), \end{aligned} \tag{1}$$

where x_L denotes the downstream link end, x_0 denotes the upstream link end, and $N^{\max}$ denotes N assuming the downstream and upstream node imposes no constraints on outflow and inflow respectively during $(t, t + \Delta t)$. Consistent with Yperman (2007, 25) and Van der Gun, Pel, and Van Arem (2017), each node can be updated with a different time window Δt. We use Δt_{x_0} and Δt_{x_L} to denote the time window sizes of the upstream and downstream node of a link respectively. To be clear, this means that every incoming link of the same node has the same Δt_{x_L} and every outgoing link of the same node has the same Δt_{x_0}. By the Courant–Friedrichs-Lewy (CFL) condition (Courant, Friedrichs, and Lewy 1928), the time window sizes of nodes must satisfy

$$\begin{cases} \Delta t_{x_0} \leq -\dfrac{L}{v'} \\ \Delta t_{x_L} \leq \dfrac{L}{u_F} \end{cases} \tag{2}$$

for all connected links, where L is the link length, u_F is the free speed, and $v' < 0$ is the wave speed in congestion.

The sending and receiving flows from Equation (1) serve as inputs to the node model of the LTM which, after resolving conflicts and applying node capacity constraints, determines the actual link inflows and outflows during such time windows, known as transition flows, forming new parts of the boundary conditions in the link models of the links connected to the node. This interaction between the link and node models is outlined in Algorithm 1.

Algorithm 1: *Calculating node flows for time window* $(t, t + \Delta t)$*, after Yperman, Logghe, and Immers (2005).*

1. Compute sending flow $S_i(t)$ for each incoming link i using the link model.
2. Compute receiving flow $R_j(t)$ for each outgoing link j using the link model.
3. Determine turning fraction $S_{ij}(t)/S_i(t)$ for each turn ij.
4. Compute transition flow $G_{ij}(t)$ for each turn ij using the node model.
5. Extend downstream boundary condition of each incoming link i with $\sum_j G_{ij}(t)$.
6. Extend upstream boundary condition of each outgoing link j with $\sum_i G_{ij}(t)$.

The extension of the LTM to variable FDs and initial conditions, as proposed in this paper, adds a third component to the link model, namely the ability to compute the densities within links. Furthermore, the sending and receiving flow algorithms are adapted to take the initial condition into account. Figure 4 illustrates the three link model components in the space–time plane: computation of within-link densities at time t, computation of the sending flow for a time window $(t, t + \Delta t_{x_L})$, and computation of the receiving flow for a time window $(t, t + \Delta t_{x_0})$. The figure also illustrates their inputs: an upstream boundary condition at location x_0, a downstream boundary condition at location x_L, and an initial condition at time t^*.

The node model on the other hand is not affected by our extension of the LTM. Despite the sending and receiving flows being calculated differently by the extended link model, the node model processes these sending and receiving flows in the same way. Any driving behaviour parameters of the node model, e.g. priorities or signal capacities, can be trivially changed during the simulation. We will therefore not discuss node models any further in this paper. The disaggregation of traffic required for step 3 of Algorithm 1 can be modelled exogenously by means of pre-specified turning fractions or endogenously with a multi-commodity LTM. Appendix 2 describes how to add support for multiple commodities to our extended LTM.

As mentioned in the introduction, the LTM can be used with either discrete or continuous time. In case of discrete time, the Δt of each node is its constant time step size. In case of continuous time, each Δt is variable and determined ad hoc. The use of continuous time requires the FD to be piecewise-linear or to be discretised as such (Bliemer and Raadsen 2018). Since the FD shape, we choose in Section

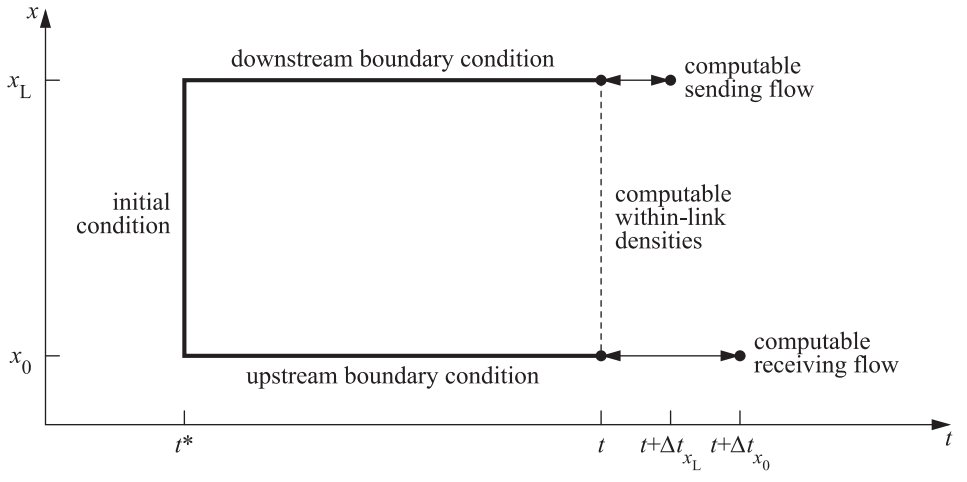

Figure 4. Illustration of the three link model components in the space–time (x, t) plane.

3.2 is generally not piecewise-linear, we opt for the discrete-time approach in this paper. For each time t^* one wishes to change the FD, we require that t^* is an integer multiple of both Δt_{x_0} and Δt_{x_L}, because the link model assumes that the FD does not change within any time step.

3. Link modelling prerequisites

In this section, we discuss the mathematical prerequisites for deriving the (extended) LTM link model, namely the used traffic flow theory and FD. The LWR traffic flow theory is introduced in Section 3.1. Our chosen FD shape is introduced in Section 3.2. Finally, Section 3.3 explains the types of shocks and fans that can occur in the solution when applying the aforementioned LWR theory and FD shape, and the impact of shocks on solution methods.

3.1. LWR traffic flow theory

As indicated in the introduction, we develop our model for the propagation of traffic on a link following LWR traffic flow theory. LWR theory traditionally is built on conservation of vehicles in the form of a scalar conservation law

$$\frac{\partial k(x,t)}{\partial t} + \frac{\partial q(x,t)}{\partial x} = 0, \tag{3}$$

where x indicates the position along the link, t indicates time, $k(x, t)$ describes the density of traffic and $q(x, t)$ describes the flow of traffic. From there, LWR theory proceeds by substituting a continuous FD of traffic flow $Q(k)$, mapping any density k to a corresponding flow q:

$$\frac{\partial k(x,t)}{\partial t} + \frac{\mathrm{d}Q(k)}{\mathrm{d}k}\frac{\partial k(x,t)}{\partial x} = 0, \quad q(x,t) = Q(k(x,t)). \tag{4}$$

Using the Lax (1957) shock admissibility or entropy condition, it has a unique solution that can be constructed using the method of characteristics. While the FD is constant, each characteristic has a constant wave speed $\mathrm{d}x/\mathrm{d}t = \mathrm{d}Q(k)/\mathrm{d}k$ and carries a constant traffic state $(k, Q(k))$. We remark it is sufficient for $\mathrm{d}Q(k)/\mathrm{d}k$ to exist only almost everywhere, by treating any problem with $k \to Q(k)$ with sharp corners as a limiting case of the problem with a similar function with smooth corners. This results in an effectively multi-valued $\mathrm{d}Q(k)/\mathrm{d}k$ at previous jumps.

Differential Equation (4) can also be reformulated into the Hamilton-Jacobi equation

$$\frac{\partial N(x,t)}{\partial t} - Q\left(-\frac{\partial N(x,t)}{\partial x}\right) = 0, \quad q(x,t) = \frac{\partial N(x,t)}{\partial t}, \quad k(x,t) = -\frac{\partial N(x,t)}{\partial x}, \tag{5}$$

which preserves both the FD and conservation of vehicles (Newell 1993). Its solution $N(x,t)$ is continuous, but is continuously-differentiable only almost everywhere, matching the solution of (4). Along each characteristic, we have

$$\partial N = Q(k)\partial t - k\partial x. \tag{6}$$

Jumps in $q(x,t)$ or $k(x,t)$ are permitted along contact discontinuities, which have characteristics run in parallel on both sides, or along shocks, which absorb characteristics from one or both sides as time t progresses. The solution may contain rarefaction waves, also known as fans, when characteristics diverge from a point on an initial or boundary condition (Evans 2002).

3.2. Smulders fundamental diagram

To solve the propagation of traffic along a link based on LWR theory, we need a specification of the FD. As suggested in the introduction, we will restrict ourselves to a specific shape to avoid introducing numerical errors within the link model itself. We introduce the FD shape here, and explain the avoidance of numerical errors in Section 4.1.

The FD shape we choose is the Smulders (1990, 117) FD. Its congested branch is linear in the flow-density plane, while its free-flow branch is linear in the speed-density plane, thus parabolic in the flow-density plane. It can be uniquely characterised by a free speed u_F, a critical speed $u_C \le u_F$, a capacity q_C and a jam density k_J. An example diagram is shown in Figure 5. Note that setting $u_C = u_F$ yields the triangular FD as a special case of the Smulders FD, and hence is also supported.

One special feature we add to this FD is that we extend its congested branch with zero flow past the jam density:

$$\forall k \ge k_J : Q(k) = 0. \tag{7}$$

Although densities exceeding jam density cannot occur in the solution if such densities are not present in the initial condition (Daganzo 2005, 192), this may be unavoidable when the FD changes during a simulation and the current traffic on the link is to be preserved, for example when a lane is closed while the link is congested.

The formulas for speed $U(k)$ and flow $Q(k)$ as functions of density k are

$$U(k) = \begin{cases} u_F - \dfrac{u_F - u_C}{k_C}k & \text{if } k \le k_C \\ v'\left(1 - \dfrac{k_J}{k}\right) & \text{if } k_C \le k \le k_J \\ 0 & \text{if } k_J \le k \end{cases}$$

$$Q(k) = kU(k) = \begin{cases} u_F k - \dfrac{u_F - u_C}{k_C}k^2 & \text{if } k \le k_C \\ v'(k - k_J) & \text{if } k_C \le k \le k_J \\ 0 & \text{if } k_J \le k \end{cases}, \tag{8}$$

where $k_C = q_C/u_C$ is the critical density. For free-flow traffic states ($k \le k_C$), the wave speed $V(k)$ as a function of density k is

$$V(k) = \frac{\mathrm{d}Q(k)}{\mathrm{d}k} = u_F - 2\frac{u_F - u_C}{k_C}k. \tag{9}$$

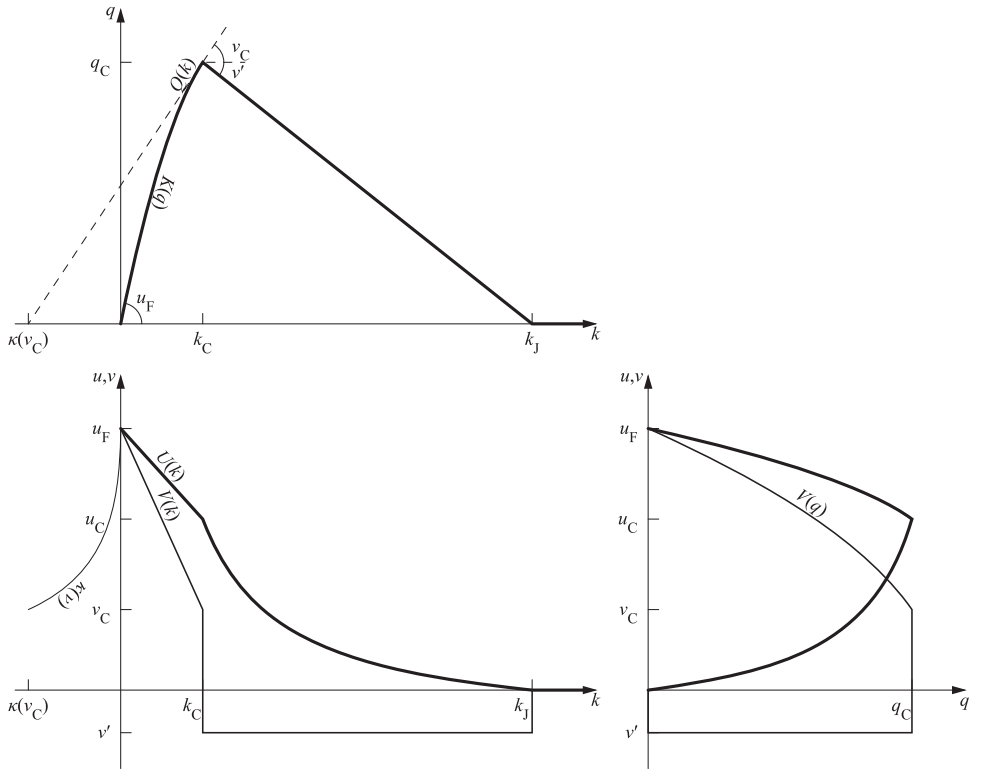

Figure 5. Smulders fundamental diagram (thick solid lines) and corresponding wave speeds (medium solid lines), including the extension beyond jam density.

After some algebraic transformations of the formulas for $Q(k)$ and $V(k)$ for the free-flow branch, we find

$$K(q) = k|_{k:Q(k)=q \wedge k<k_C} = \begin{cases} \dfrac{q}{u_F} & \text{if } u_F = u_C \\ \dfrac{1}{2}\dfrac{k_C}{u_F - u_C}\left(u_F - \sqrt{{u_F}^2 - 4\dfrac{u_F - u_C}{k_C}q}\right) & \text{otherwise} \end{cases}$$

$$V(q) = V(K(q)) = \sqrt{{u_F}^2 - 4\frac{u_F - u_C}{k_C}q} \tag{10}$$

describing the density $K(q)$ and wave speed $V(q)$ as functions of flow q. We abbreviate the critical wave speed $v_C = V(k_C) = V(q_C) = 2u_C - u_F$. The intersection $\kappa(v) \leq 0$ of a tangent line of wave speed $v \in [v_C, u_F]$ to the free-flow branch in the flow-density plane with the density axis is

$$\kappa(v) = K(q) - \frac{q}{v}\Big|_{q:V(q)=v} = \begin{cases} 0 & \text{if } u_F = u_C \\ \dfrac{1}{4}\dfrac{k_C}{u_F - u_C}\left(2u_F - \dfrac{u_F^2}{v} - v\right) & \text{otherwise.} \end{cases} \tag{11}$$

3.3. Types of shocks and fans

Before proceeding to develop the LTM link model using the LWR theory and FD shape described above, it is helpful to understand what types of shocks and fans may occur in the analytical solutions of links.

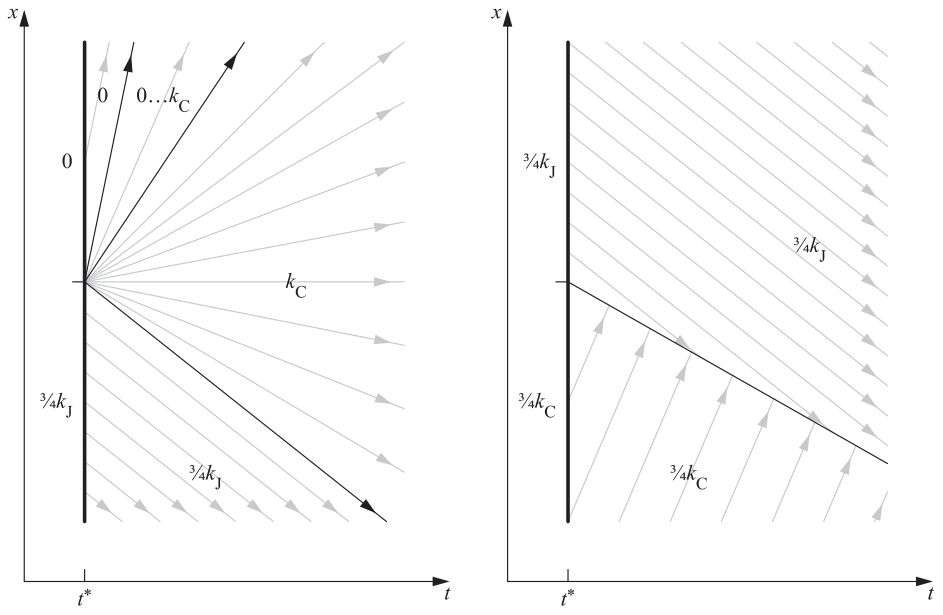

Figure 6. Example Riemann problems showing an acceleration fan (left) and a deceleration shock (right).

This subsection explains the possible types of shocks and fans, as well as the impact of shocks on solution methods. Each type is illustrated with an example Riemann problem.

In most traffic flow applications, $k \to Q(k)$ is concave. With a concave FD in traffic flow, rarefaction waves occur when traffic accelerates (acceleration fans) whereas shocks occur when traffic decelerates (deceleration shocks). This is illustrated in Figure 6 with the solutions (densities) and characteristics (arrows) of example Riemann problems.

In Hamilton-Jacobi Equation (5), the so-called Hamiltonian $\partial N/\partial x \to -Q(-\partial N/\partial x)$ is then convex, which allows for direct solution of any point $N(x,t)$ from initial and boundary conditions by applying variational theory (Evans 2002; Daganzo 2005). Whenever there are multiple candidate characteristics from the initial and boundary conditions passing through point (x,t), variational theory tells us that the correct solution $N(x,t)$ is the minimum of all values corresponding to those candidate characteristics. This Newell–Luke minimum principle (Luke 1972; Newell 1993) allows us to solve $N(x,t)$ without explicitly keeping track of any shocks. In this process, the variational theory allows us to include candidate characteristics that do not carry the true traffic state at the initial or boundary condition, but some other traffic state, as such inclusion will not affect the minimum $N(x,t)$.

The FD from the previous subsection is however only concave for $k < k_J$. The extension of the congested branch beyond jam density gives rise to additional types of possible shocks and fans. Specifically, the solution can now also involve deceleration fans with constant traffic state $(k_J, 0)$ and acceleration shocks with shock speeds slower than the wave speed in congestion $v' = q_C/(k_C - k_J)$. Examples of such acceleration shocks and deceleration fans are illustrated in the Riemann problems of Figure 7. These possibilities are in addition to the acceleration fans and deceleration shocks that can normally occur in a solution with a concave FD. The solution may even involve combined shocks and fans, as illustrated in Figure 8.

The introduction of acceleration shocks has an important consequence for solution methods based on variational theory: we can no longer apply the Newell–Luke minimum principle to resolve any conflicts between candidate characteristics. Yet, we still have that all candidate characteristics pose some sort of constraints on N. Using logical reasoning about the traffic processes beneath a pair of conflicting candidate characteristics, we can still deduce whether the candidate characteristic yielding minimum

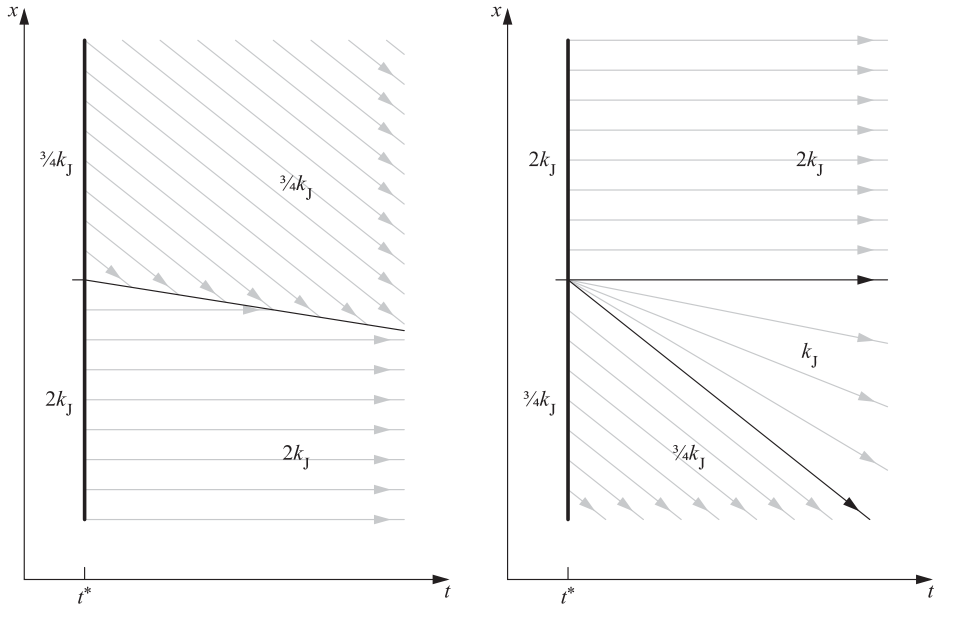

Figure 7. Example Riemann problems showing an acceleration shock (left) and a deceleration fan (right).

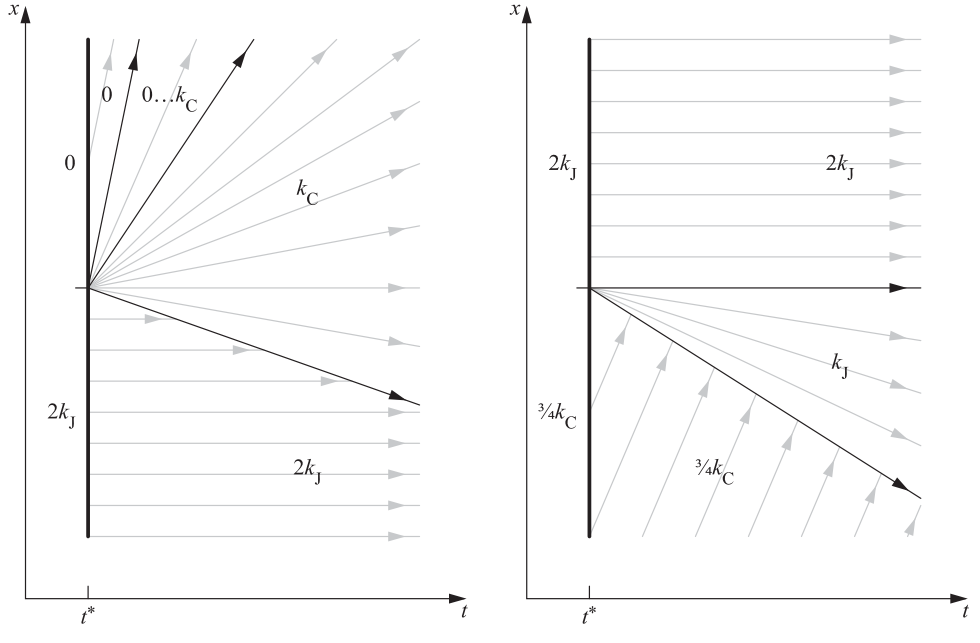

Figure 8. Example Riemann problems showing a combined acceleration shock and acceleration fan (left) and a combined deceleration shock and deceleration fan (right).

N wins the conflict or whether the one yielding maximum *N* wins. Specifically, in case of a potential deceleration shock, both candidate characteristics form upper bounds on *N*, so that the minimum *N* wins. Likewise, in case of a potential acceleration shock, they form lower bounds on *N*, so that the maximum *N* wins. Overall, we thus can still construct the solution using variational theory, as long as we

are aware of the nature of the comparison of candidate characteristics. The link model formulation in the next section takes advantage of this.

4. Link model formulation

With the LWR theory and FD specification from Section 3, we now develop the link model in this section. This section is structured as follows. Section 4.1 discusses the shape of the boundary and initial conditions. Using these shapes, Section 4.2 outlines the general solution method for all link model components. Then, Section 4.3 derives a procedure for computing the within-link densities, Section 4.4 derives a procedure for computing the receiving flow, and Section 4.5 derives a procedure for computing the sending flow.

4.1. Shapes of boundary and initial conditions

Since the LTM assumes link inflows and link outflows to be constant for the duration of some chosen time windows, the upstream and downstream boundary conditions of the link consist of piecewise-constant flows, with each piece formed by the solution of the node model of the LTM. The cumulative vehicle number N will thus be piecewise-linear in t. Note that if this does not hold for the algebraic network-level solution, the LTM results will be a numerical approximation. This approximation is imposed by the structure of the LTM and also occurs in other discrete-time traffic simulation models.

The shape of initial conditions is chosen to be restricted for a consistency reason. The initial density profile of a link must be piecewise-linear in x (that is, along the link), with permitted jumps. Thus, in combination with the Smulders FD, in general the initial cumulative vehicle number N will be piecewise-parabolic in x. The pieces need not have equal spatial length. Note that piecewise-constant, constant and zero density profiles are special cases of the piecewise-linear density profile.

The consistency reason is that the shape of the initial condition corresponds with the possible shapes of within-link traffic state profiles that can be produced through simulation with the Smulders FD shape and piecewise-constant boundary flows. This consistency is proven in Lemma 4.1.1 and Theorem 4.1.1, provided that a minimum amount of time has passed since the initial condition. We use $L = x_L - x_0$ to denote link length, i.e. the distance from the upstream end x_0 to the downstream end x_L.

Lemma 1: *Along a characteristic with wave speed $\partial x/\partial t \in [v_C, u_F]$, it holds that $\partial N = -\partial x \kappa(\partial x/\partial t)$. This expression is parabolic in ∂x.*

Proof: Rearranging Equation (6), we find

$$\partial N = Q(k)\partial t - k\partial x = \left(Q(k)\frac{\partial t}{\partial x} - k\right)\partial x = -\left(k - \frac{Q(k)}{\partial x/\partial t}\right)\partial x. \tag{12}$$

To be a characteristic, traffic state $(k, Q(k))$ must match with wave speed $\partial x/\partial t$. Assuming $(k, Q(k))$ is a free-flow traffic state ($k \leq k_C$) with corresponding wave speed $\partial x/\partial t \in [v_C, u_F]$, the factor between parentheses in Equation (12) equals the definition of $\kappa(\partial x/\partial t)$ in Equation (11). After substitution, we get

$$\partial N = -\partial x \kappa\left(\frac{\partial x}{\partial t}\right) = \tfrac{1}{4}\frac{{u_F}^2 k_C}{u_F - u_C}\partial t - \tfrac{1}{2}\frac{u_F k_C}{u_F - u_C}\partial x + \tfrac{1}{4}\frac{k_C}{u_F - u_C}\frac{\partial x^2}{\partial t} \tag{13}$$

which is parabolic in ∂x. ■

Theorem 1: *With N piecewise-parabolic in x at the initial condition, and N piecewise-linear in t at the upstream and downstream boundary conditions, L/v_C or more time later, N is again piecewise-parabolic in x.*

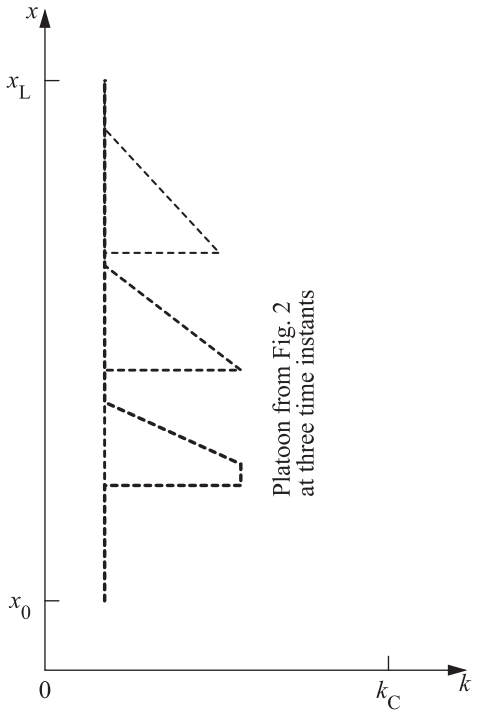

Figure 9. Density k versus location x at various times for the platoon example from Figure 2.

Proof: All traffic states within the link at the target time must have been carried there by characteristics originating from the initial and boundary conditions. Characteristics emanated from the downstream boundary condition result in N being piecewise-linear in x, since N is piecewise-linear in t at the boundary and no rarefaction waves are possible. Characteristics emanated from the initial condition cannot result in traffic states with $k < k_C$ as those characteristics leave the downstream link end within L/v_C time. Because of the shape of the FD for $k \geq k_C$, rarefaction waves will carry a constant traffic state of either (k_C, q_C) or $(k_J, 0)$, resulting in N being linear in x. Other characteristics will simply translate the initial condition, which has N piecewise-parabolic in x. Finally, characteristics emanated from the upstream boundary condition will carry constant traffic states that result in N piecewise-linear in x, unless they are part of rarefaction waves that, based on Lemma 4.4.1, result in N parabolic in x (e.g. Figure 9 shows $k = -\partial N/\partial x$ linear in x). Combining all pieces from all characteristics completes the proof.

■

Theorem 4.1.1 implies we can use the same procedure for applying initial conditions at the start of a simulation as we can for changing the FD, which involves computing and preserving the current within-link density profile. Thus, we can and will develop an exact procedure for this computation, so that no (new) numerical errors are introduced. It implies a minimum time of L/v_C between the last application of an initial condition to the link and the computation of within-link densities. In practice, this will pose a limit on, e.g. how frequently the FD of a link can be changed during a simulation. If needed, this limitation can always be circumvented by splitting long links into shorter ones.

The above piecewise descriptions of the boundary and initial conditions are put in the mathematical form in Table 1. Each boundary condition piece AB is specified by a start time t_A, an end time t_B, a start cumulative N_A, and an end cumulative N_B. Each initial condition piece AB is specified by an upstream location x_A, a downstream location x_B, an upstream cumulative N_A, a downstream

Table 1. Piecewise descriptions of the boundary and initial conditions.

	Downstream boundary condition	Initial condition	Upstream boundary condition
Space–time illustration	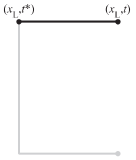		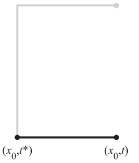
Space–time domain	$\{x_L\} \times [t^*, t]$	$[x_0, x_L] \times \{t^*\}$	$\{x_0\} \times [t^*, t]$
Piece parameters	t_A, t_B, N_A, N_B	$x_A, x_B, N_A, N_B, f_{AB}$	t_A, t_B, N_A, N_B
Piece space–time illustration		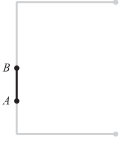	
Piece space–time domain	$\{x_L\} \times [t_A, t_B]$	$[x_A, x_B] \times \{t^*\}$	$\{x_0\} \times [t_A, t_B]$
Piece cumulative N	$N(x_L, \tau) = N_{AB}(\tau) = \frac{(t_B-\tau)N_A+(\tau-t_A)N_B}{t_B-t_A}$	$N(x, t^*) = N_{AB}(x) = \frac{(x_B-x)N_A+(x-x_A)N_B}{x_B-x_A} - f_{AB}\frac{(x_B-x)(x-x_A)}{2}$	$N(x_0, \tau) = N_{AB}(\tau) = \frac{(t_B-\tau)N_A+(\tau-t_A)N_B}{t_B-t_A}$
Piece flow $q = \partial N/\partial t$	$q(x_L, \tau) = q_{AB} = \frac{N_B-N_A}{t_B-t_A}$	$q(x, t^*) = Q(k(x, t^*))$	$q(x_0, \tau) = q_{AB} = \frac{N_B-N_A}{t_B-t_A}$
Piece density $k = -\partial N/\partial x$	$k(x_L, \tau) \overset{\text{assumed}}{=} k_J + \frac{q_{AB}}{v'}$	$k(x, t^*) = \frac{N_A-N_B}{x_B-x_A} + f_{AB}\frac{(x_B-x)-(x-x_A)}{2}$ $k_{A^+} = \lim_{x \downarrow x_A} k(x, t^*) = \frac{N_A-N_B}{x_B-x_A} + f_{AB}\frac{x_B-x_A}{2}$ $k_{B^-} = \lim_{x \uparrow x_B} k(x, t^*) = \frac{N_A-N_B}{x_B-x_A} - f_{AB}\frac{x_B-x_A}{2}$	$k(x_0, \tau) \overset{\text{assumed}}{=} K(q_{AB})$
Piece second spatial derivative $-\partial k/\partial x = \partial^2 N/\partial x^2$	$-\frac{\partial k}{\partial x}(x_L, \tau) = 0$	$-\frac{\partial k}{\partial x}(x, t^*) = f_{AB}$	$-\frac{\partial k}{\partial x}(x_0, \tau) = 0$

cumulative N_B, and a second derivative of the cumulative over space f_{AB}. Because of Theorem 4.1.1, computed within-link density profiles can be described using the same piecewise formulation as the initial condition.

4.2. General solution method

Now that the shapes of the boundary and initial conditions and within-link density profiles have all been determined, we proceed with developing algorithms for the three link model components. These components are responsible for the computation of the within-link density profile, the computation of constraints on future link inflow that determine the receiving flow, and the computation of constraints on future link outflow that determine the sending flow. All three components follow the same general solution procedure, which can be summarised as follows:

1. Iterate over the pieces of the boundary and initial conditions in counter-clockwise direction in the space–time plane in, starting with the downstream boundary.
2. Analyse how candidate characteristics emanated from the current piece or point affect the solution.
3. Apply the relevant candidate characteristics to the solution, resolving any conflicts with previous candidate characteristics in a pre-specified way.

If all candidate characteristics relevant to the solution are considered, all relevant real characteristics must be among the candidates. If the conflicts between candidate characteristics are also resolved correctly, the eventually resulting candidate characteristics must be real characteristics and our resulting solution must thus be correct. Because the FD from Section 3.2 is not entirely concave in the flow-density plane, we explicitly consider the nature of the candidate characteristics we are comparing as proposed in Section 3.3.

Note that the conflict resolution step looks for conflicts between two sets of candidate characteristics: the previous candidates and the new candidates. The output is a new, merged set of candidate characteristics with conflicts resolved. In this resolution process, we not only remove multivaluedness of N in the candidate solution but also maintain continuity of N in the candidate solution by eliminating crossing candidate characteristics. This is permitted because characteristics cannot cross, and greatly simplifies the resolution process. Namely, in case of a conflict, the merging of both input sets can only introduce one new shock in the output set, with candidate characteristics from each one input set on one side of the new shock. Only if one input set fully dominates the other, the output set equals this input set and no new shock is introduced.

To ensure all candidate characteristics possibly affecting the link are taken into account, the traffic states on the downstream boundary are assumed to be on the congested branch of the FD and the traffic states of the upstream boundary are assumed to be on the free-flow branch of the FD. These assumptions are indicated in Table 1 and are based on the need for candidate characteristics to enter the link. The kind of candidate characteristics emanated from a piece of the initial condition depend on whether the density is lower than the critical density (Free-flow), between the critical density and jam density (Congested), or exceeding the jam density (Jammed). We will treat these cases separately. Therefore, ensure that all the pieces AB satisfy

$$\underbrace{\forall x \in (x_A, x_B) : k(x, t^*) \leq k_C}_{\text{type Free - flow}} \quad \vee \quad \underbrace{\forall x \in (x_A, x_B) : k_C \leq k(x, t^*) \leq k_J}_{\text{type Congested}} \quad \vee \quad \underbrace{\forall x \in (x_A, x_B) : k_J \leq k(x, t^*)}_{\text{type Jammed}}, \tag{14}$$

by splitting unclassifiable pieces into smaller pieces wherever the density passes k_C or k_J.

In the following three subsections, each component is discussed individually.

4.3. Computing the within-link density profile

We start in this subsection with the computation of within-link densities. Although the proof of Theorem 4.1.1 already hints at which candidate characteristics to take into account to compute the within-link densities, it does not yet offer formulas for them nor specifies how to resolve conflicts between characteristics that result in multi-valued N. We will now develop the method in detail, calculating the within-link density profile at (current) time t, assuming a time difference with the initial condition of at least L/v_C in accordance with Theorem 4.1.1. The output consists of an exact, piecewise description of $N(x, t)$ on $[x_0, x_L] \times \{t\}$, without any discretisation of space within the link, in the same piecewise format as the initial condition.

All candidate characteristics relevant to the computation of the within-link density profile are described in Table 2. Each row represents a class of relevant candidate characteristics emanating from different pieces and points of the boundary and initial conditions. Space–time visualisations of

Table 2. Candidate characteristics affecting the within-link density profile.

Space–time illustration	Candidate characteristics beginnings and endings	Ending cumulative N and second spatial derivative $-\partial k/\partial x = \partial^2 N/\partial x^2$	Conflict resolution
[1] Piece of downstream boundary condition: 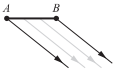	$\{x_L\} \times [t_A, t_B] \rightarrow$ $\begin{bmatrix} \max(x_0, x_L + (t - t_A)v'), \\ x_L + (t - t_B)v' \end{bmatrix} \times \{t\}$	$N(x,t) = N\left(x_L, t + \frac{x_L - x}{v'}\right) + (x_L - x)k_J$ $-\frac{\partial k}{\partial x}(x,t) = 0$	N/A
[2] Consecutive pieces of initial condition, type Congested or Jammed upstream of type Free-flow: 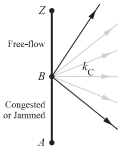	$\{x_B\} \times \{t^*\} \rightarrow$ $\begin{bmatrix} \max(x_0, x_B + (t - t^*)v'), \\ x_L \end{bmatrix} \times \{t\}$	$N(x,t) = N_B + (t - t^*)q_C - (x - x_B)k_C$ $-\frac{\partial k}{\partial x}(x,t) = 0$	⤒ min
[3] Piece of initial condition, type Congested: 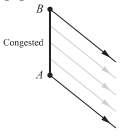	$[x_A, x_B] \times \{t^*\} \rightarrow$ $\begin{bmatrix} \max(x_0, x_A + (t - t^*)v'), \\ x_B + (t - t^*)v' \end{bmatrix} \times \{t\}$	$N(x,t) = N(x - (t - t^*)v', t^*) + (t - t^*)v'k_J$ $-\frac{\partial k}{\partial x}(x,t) = f_{AB}$	N/A
[4] Piece of initial condition, type Jammed: 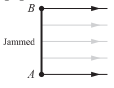	$[x_A, x_B] \times \{t^*\} \rightarrow$ $[x_A, x_B] \times \{t\}$	$N(x,t) = N(x,t^*)$ $-\frac{\partial k}{\partial x}(x,t) = f_{AB}$	⤒ max
[5] Consecutive pieces of initial condition, type Free-flow or Congested upstream of type Jammed: 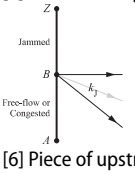	$\{x_B\} \times \{t^*\} \rightarrow$ $\begin{bmatrix} \max(x_0, x_B + (t - t^*)v'), \\ x_B \end{bmatrix} \times \{t\}$	$N(x,t) = N_B + (x - x_B)k_J$ $-\frac{\partial k}{\partial x}(x,t) = 0$	⤒ max
[6] Piece of upstream boundary condition: 	$\{x_0\} \times [t_A, t_B] \rightarrow$ $\begin{bmatrix} x_0 + (t - t_B)V(q_{AB}), \\ \min(x_0 + (t - t_A)V(q_{AB}), x_L) \end{bmatrix} \times \{t\}$	$N(x,t) = \frac{(t_B - t)N_A + (t - t_A)N_B}{t_B - t_A} - (x - x_0)K(q_{AB})$ $-\frac{\partial k}{\partial x}(x,t) = 0$	⤒ min
[7] Consecutive pieces of upstream boundary condition: 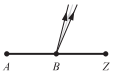	$\{x_0\} \times \{t_B\} \rightarrow$ $\begin{bmatrix} x_0 + (t - t_B)V(q_{BZ}), \\ \min(x_0 + (t - t_B)V(q_{AB}), x_L) \end{bmatrix} \times \{t\}$	$N(x,t) = N_B - (x - x_0)\kappa\left(\frac{x - x_0}{t - t_B}\right)$ $-\frac{\partial k}{\partial x}(x,t) = \frac{1}{2}\frac{k_C}{u_F - u_C}(t - t_B)^{-1}$	⤒ min

how these characteristics emanate from the boundary and initial conditions are provided in the first column, including the naming of points used later in the row.

The second column gives a mathematical description of the space–time origins of the candidate characteristics as well as their destinations at time t when the within-link density profile is calculated. These destination sets are intersected with $[x_0, x_L] \times \{t\}$ to eliminate candidate characteristics that have left the link before time t and hence do not affect the within-link densities at that time.

For the remaining candidate characteristics, the third column gives the formulas for the corresponding values of cumulative N at their destinations, obtained by integrating N over the candidate characteristic. The formula for its second spatial derivative $\partial^2 N/\partial x^2 = -\partial k/\partial x$ is also listed; due to Theorem4.1.1 its value is constant. Together, the spatial endpoints of the destinations in the second column and the formulas in the third column allow construction of a candidate piece of the piecewise-parabolic solution.

Finally, the fourth column indicates how any conflicts with previously found candidate pieces are to be resolved, assuming candidate characteristics are considered in counter-clockwise order as described in Section 4.2:

- 'N/A' means that no conflicts are possible;
- 'min' means that the candidate characteristics yielding minimum N should be kept;
- 'max' means that the candidate characteristics yielding maximum N should be kept.

If there are conflicts to be resolved, the '$\overline{\uparrow}$' symbol indicates that the new candidate characteristics corresponding to this row of the table must be on the upstream side of a newly created shock. This specifies the searching direction for the possible shock through the previous candidate pieces. The location of any shock between the new candidate piece and a previous candidate piece between their spatial endpoints is to be determined with the quadratic formula. If a shock is found, the previous piecewise solution is truncated to the shock location before the new (truncated) piece is added to the solution. Appendix A.1 describes this process in more detail.

We will now describe each row of Table 2:

[1] Each piece of the downstream boundary condition is assumed to be congested and hence generates candidate characteristics with wave speed v', representing a constant congested traffic state. Because all these characteristics run in parallel, no conflict occurs.

[2] Characteristics from pieces of the initial condition of type Free-flow can no longer affect the link interior at time t because they reach the downstream link end before that time. However, if such a piece has another piece of type Congested or Jammed upstream of it, the acceleration fan emanated from between these pieces can affect the solution. This fan carries the capacity state (k_C, q_C). Its upstream end is limited by wave speed v', while its downstream end can always reach the downstream link end. If the fan conflicts with any previous candidate characteristics, the fan represents an upper bound on the flow into the congestion ($k \geq k_C$) represented by the previous candidate characteristics. A conflict is thus resolved by taking minimum N, possibly resulting in a deceleration shock.

[3] A piece of the initial condition of type Congested emanates candidate characteristics with wave speed v', translating the traffic states from the initial condition and therefore preserving the second spatial derivative. They run parallel to previous candidate characteristics and hence no conflicts occur.

[4] A piece of the initial condition of type Jammed emanates candidate characteristics with zero speed. If these conflict with previous candidate characteristics, the previous candidates represent the outflow ($k \leq k_J$) from this jam. A conflict is thus resolved by taking maximum N, possibly resulting in an acceleration shock.

[5] If a piece of the initial condition of type Jammed has another piece of type Free-flow or Congested upstream of it, a deceleration fan is emanated from between the pieces. This fan carries the jammed state $(k_J, 0)$. Its wave speeds range from v' to zero. Like the previous row, a conflict is resolved by taking maximum N, possibly resulting in an acceleration shock.

[6] Each piece of the upstream boundary condition is assumed to be free-flow and hence generates candidate characteristics representing a constant free-flow traffic state, with the wave speed from Equation (10). They form an upper bound on flow into downstream traffic states in case of conflict, which is thus resolved by taking minimum N, possibly resulting in a deceleration shock.

[7] Between two consecutive pieces of the upstream boundary condition, an acceleration fan can be emanated and equation determine the cumulative and second spatial derivative at its destination. Like the previous row, a conflict is resolved by taking minimum N, possibly resulting in a deceleration shock.

4.4. Computing the receiving flow

The receiving flow is the maximum flow that can enter the link at x_0. At the start of the simulation, the downstream boundary condition is unknown, thus it is clearly not possible to determine all link inflow constraints at once. We shall assume that the downstream boundary condition is only known up to the current time t, which, by the CFL condition, suffices to compute any constraints on future cumulative inflow until $t - L/v'$. Equation (1) converts these cumulative inflow constraints into the receiving flow.

The main feature of the computation of the receiving flow in this subsection and the sending flow in the next subsection is that they consider the implications of the initial and boundary conditions for all future cumulative inflow and outflow simultaneously, instead of looking at only one time step at a time. This means that the bulk of the work in Algorithm 1 is done in steps 5 and 6 rather than steps 1 and 2, similar to Gentile and Papola (2009b) and Gentile (2010). This increases the computational efficiency compared to Van der Gun, Pel, and Van Arem (2017) because it avoids the need to iterate over all possible wave speeds every time step.

Similar to Section 4.3, Table 3 lists all candidate characteristics relevant for future inflow constraints. The first column provides a space–time visualisation of the characteristics. The second column indicates the space–time origins and destinations of the characteristics. The third column gives formulas for the destination cumulative N and its second time derivative $\partial^2 N/\partial t^2 = \partial q/\partial t$. Because the second time derivative is always constant, it is possible to compute an exact, piecewise-parabolic description of the cumulative inflow constraints. However, since the calculation of receiving flows only needs to know the cumulative inflow constraint at a finite set of times, it is more convenient to directly calculate the cumulative inflow constraint at these specific times only. The fourth column indicates whether to keep the minimum or maximum N in case of conflicts. The '$\twoheadrightarrow$' symbol specifies the searching direction for shocks, indicating that the new candidate characteristics corresponding to this row will be on the before side of any shock with previous candidate characteristics (see Appendix 3).

We will now describe each row of Table 3:

[1] Assuming the link outflow after current time t would be zero, the assumed future downstream boundary condition generates candidate characteristics with wave speed v' carrying traffic state $(k_J, 0)$. Because of satisfaction of the CFL condition, this assumption does not affect the relevant part of the solution ($t + \Delta t_{x_0} \leq t - L/v'$) and applying these candidate characteristics is thus entirely optional. We do include this row for two reasons. First, it makes it easier to update the cumulative inflow constraints when new pieces of the downstream boundary condition become known, without redoing the entire computation. This is discussed further below. Secondly, it ensures the cumulative inflow constraints always end in constant N (row [1] or row [5]), allowing the constraints applying to an infinite future to be more easily stored in finite computer memory.

[2] Each piece of the downstream boundary condition produces congested traffic states with wave speed v'. No conflict occurs.

[3] Characteristics from between pieces of the initial conditions of type Congested or Jammed and type Free-flow form a fan carrying capacity state (k_C, q_C), between wave speeds v' and v_C. In case of conflict with previous candidate characteristics, this fan represents inflow into previous congestion ($k \geq k_C$). A conflict is thus resolved by taking minimum N.

[4] Each piece of the initial condition of type Congested produces congested traffic states with wave speed v'. No conflict occurs.

[5] The upstream end of a piece of the initial condition of type Jammed generates a fan of candidate characteristics carrying traffic state $(k_J, 0)$, between wave speeds v' and zero. In case of conflict, previous characteristics represent the outflow ($k \leq k_J$) from this jam fan. A conflict is thus resolved by taking maximum N.

[6] From the last known upstream point (x_0, t), one candidate characteristic carrying capacity state (k_C, q_C) restricts future inflow. In case of conflict, this represents inflow into previous congestion

Table 3. Candidate characteristics affecting future link inflow.

Space–time illustration	Candidate characteristics beginnings and endings	Ending cumulative N and second time derivative $\partial q/\partial t = \partial^2 N/\partial t^2$	Conflict resolution
[1] Most recent downstream point: 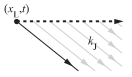	$\{x_L\} \times [t, \infty) \rightarrow$ $\{x_0\} \times \left[t - \frac{L}{v'}, \infty\right)$	$N(x_0, \tau) = N(x_L, t) + Lk_J$ $\frac{\partial q}{\partial \tau}(x_0, \tau) = 0$	N/A
[2] Piece of downstream boundary condition: 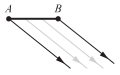	$\{x_L\} \times [t_A, t_B] \rightarrow$ $\{x_0\} \times \left[\begin{array}{c} t_A - \frac{L}{v'}, \\ t_B - \frac{L}{v'} \end{array}\right]$	$N(x_0, \tau) = N\left(x_L, \tau + \frac{L}{v'}\right) + Lk_J$ $\frac{\partial q}{\partial \tau}(x_0, \tau) = 0$	N/A
[3] Consecutive pieces of initial condition, type Congested or Jammed upstream type Free-flow: 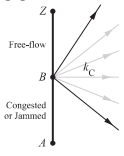	$\{x_B\} \times \{t^*\} \rightarrow$ $\{x_0\} \times \left[t^* - \frac{x_B - x_0}{v'}, \infty\right)$	$N(x_0, \tau) = N_B + (\tau - t^*)q_C + (x_B - x_0)k_C$ $\frac{\partial q}{\partial \tau}(x_0, \tau) = 0$	$\twoheadrightarrow$ min
[4] Piece of initial condition, type Congested: 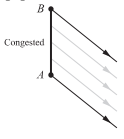	$[x_A, x_B] \times \{t^*\} \rightarrow$ $\{x_0\} \times \left[\begin{array}{c} t^* - \frac{x_A - x_0}{v'}, \\ t^* - \frac{x_B - x_0}{v'} \end{array}\right]$	$N(x_0, \tau) = N(x_0 - (\tau - t^*)v', t^*) - (\tau - t^*)v'k_J$ $\frac{\partial q}{\partial \tau}(x_0, \tau) = v'^2 f_{AB}$	N/A
[5] Piece of initial condition, type Jammed: 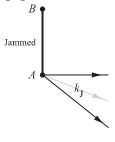	$\{x_A\} \times \{t^*\} \rightarrow$ $\{x_0\} \times \left[t^* - \frac{x_A - x_0}{v'}, \infty\right)$	$N(x_0, \tau) = N_A + (x_A - x_0)k_J$ $\frac{\partial q}{\partial \tau}(x_0, \tau) = 0$	$\twoheadrightarrow$ max
[6] Most recent upstream point: 	$\{x_0\} \times \{t\} \rightarrow$ $\{x_0\} \times [t, \infty)$	$N(x_0, \tau) = N(x_0, t) + (\tau - t)q_C$ $\frac{\partial q}{\partial \tau}(x_0, \tau) = 0$	$\twoheadrightarrow$ min

($k \geq k_C$). A conflict is thus resolved by taking minimum N. This row is equivalent to limiting the receiving flow to $q_C \Delta t_{x_0}$.

We now discuss how the cumulative inflow constraints resulting from this computation can be updated when new pieces of the downstream and upstream boundary conditions become known in steps 5 and 6 of Algorithm 1. For a new piece of the upstream boundary condition, this is as simple as applying row [6] again.

Due to the previous assumption of zero flow in row [1], a new piece of the downstream boundary condition can only relax the constraints on future inflow. However, the upper bounds posed by rows [3] and [6] still apply. Based on the mathematical principle

$$\min(a, \max(b, c)) = \max(\min(a, b), \min(a, c)), \tag{15}$$

we can update the previously calculated cumulative inflow constraints by taking the maximum N, provided that the minimum N operations associated with rows [3] and [6] are first applied to the updated candidate characteristics from rows [1] and [2]. This does not require iterating over the initial condition

on every update of the downstream boundary condition: since all constraints based on rows [3] have identical flow q_C, one is the most constraining for every update, requiring only that one to be applied. The searching direction for the update is '↞'.

4.5. Computing the sending flow

The sending flow is the maximum flow that can leave the link at x_L. At the start of the simulation, the upstream boundary condition is unknown, thus it is clearly not possible to determine all link outflow constraints at once. We shall assume that the upstream boundary condition is only known up to the current time t, which, by the CFL condition, suffices to compute any constraints on future cumulative outflow until $t + L/u_F$. Equation (1) converts these cumulative outflow constraints into the sending flow.

Similar to the last two subsections, Table 4 lists all candidate characteristics relevant for future outflow constraints. Unlike Table 3, the third column does not list the second time derivative. The reason for this is that it is not always constant; a piecewise-parabolic description of the cumulative outflow constraints thus cannot be constructed. Since the calculation of sending flows only needs to know the cumulative outflow constraint at a finite set of times, one directly calculates the cumulative outflow constraint at these specific times only. Because the calculation of outflow constraints only involves candidate characteristics associated with the concave free-flow branch of the FD, all conflicts are resolved by taking minimum N. The searching direction for shocks is always '↞', meaning that new candidate characteristics will be on the after side of a shock with previous candidate characteristics. An example is provided in Appendix A.2.

We will now describe each row of Table 4:

[1] From the last known downstream point (x_L, t), one candidate characteristic carrying capacity state (k_C, q_C) restricts future outflow. This row is equivalent to limiting the sending flow to $q_C \Delta t_{x_L}$.

[2] A piece of the initial condition of type Free-flow emits candidate characteristics that either diverge ($\partial k/\partial x < 0$), converge ($\partial k/\partial x > 0$), or run in parallel ($\partial k/\partial x = 0$). Within the fan, the candidate characteristic ending at (x_L, τ) originates from the point $(X(\tau), t^*)$, where $X(\tau)$ is the solution of $x_L - X(\tau) = (\tau - t^*)V(k(X(\tau), t^*))$. If in case of convergence, the point of convergence is upstream of x_L, the link outflow is unaffected.

[3] A fan of candidate characteristics can be emanated from between two pieces of the initial condition of type Free-flow. If the density upstream of the point does not exceed the density downstream of the point, no fan occurs and the link outflow is unaffected.

[4] Similarly, a fan of candidate characteristics is emanated from between two pieces of the initial condition of type Congested or Jammed and type Free-flow. For the infinite part of the fan carrying constant capacity state (k_C, q_C), only the first point in time needs to be applied: row [1] will then ensure the capacity state is continued into later sending flows.

[5] A fan of candidate characteristics can be emanated from between a piece of the initial condition of type Free-flow and an adjacent piece of the upstream boundary condition. If the wave speed downstream of the point does not exceed the wave speed after the point, no fan occurs.

[6] Each piece of the upstream boundary condition generates candidate characteristic carrying a constant free-flow traffic state, with corresponding wave speed.

[7] A fan of candidate characteristics can be emanated from between two pieces of the upstream boundary condition. If the flow after the point does not exceed the flow before the point, no fan occurs.

When a new piece of the downstream boundary condition becomes available in step 5 of Algorithm 1, row [1] can simply be applied again to update the cumulative outflow constraints. When a new piece of the upstream boundary condition becomes known in step 6 of Algorithm 1, one can update the constraints by applying either row [5] or [7], followed by row [6] for the new piece.

Table 4. Candidate characteristics affecting future link outflow.

Space–time illustration	Candidate characteristics beginnings and endings	Ending cumulative N	Conflict resolution
[1] Most recent downstream point: 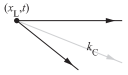	$\{x_L\} \times \{t\} \rightarrow$ $\{x_L\} \times [t, \infty)$	$N(x_L, \tau) = N(x_L, t) + (\tau - t) q_C$	N/A
[2] Piece of initial condition, type Free-flow: 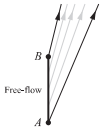	$[x_A, x_B] \times \{t^*\} \rightarrow$ $\{x_L\} \times \begin{bmatrix} t^* + \frac{x_L - x_B}{V(k_{B^-})}, \\ t^* + \frac{x_L - x_A}{V(k_{A^+})} \end{bmatrix}$	$N(x_L, \tau) = N(X(\tau), t^*) - (x_L - X(\tau))\kappa\left(\frac{x_L - X(\tau)}{\tau - t^*}\right)$ where $X(\tau) = \frac{x_L - (\tau - t^*)\left(u_F + \left(\frac{N_A - N_B}{x_B - x_A} + f_{AB}\frac{x_A + x_B - 2x_0}{2}\right)\frac{\mathrm{d}V(k)}{\mathrm{d}k}\right)}{1 - (\tau - t^*) f_{AB}\frac{\mathrm{d}V(k)}{\mathrm{d}k}}$ with $\frac{dV(k)}{dk} = -2\frac{u_F - u_C}{k_C}$	↤ min
[3] Consecutive pieces of initial condition, type Free-flow upstream of type Free-flow: 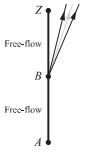	$\{x_B\} \times \{t^*\} \rightarrow$ $\{x_L\} \times \begin{bmatrix} t^* + \frac{x_L - x_B}{V(k_{B^+})}, \\ t^* + \frac{x_L - x_B}{V(k_{B^-})} \end{bmatrix}$	$N(x_L, \tau) = N_B - (x_L - x_B)\kappa\left(\frac{x_L - x_B}{\tau - t^*}\right)$	↤ min
[4] Consecutive pieces of initial condition, type Congested or Jammed upstream of type Free-flow: 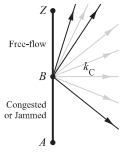	$\{x_B\} \times \{t^*\} \rightarrow$ $\{x_L\} \times \left[t^* + \frac{x_L - x_B}{V(k_{B^+})}, \infty\right)$	$N(x_L, \tau) = \begin{cases} N_B - (x_L - x_B)\kappa\left(\frac{x_L - x_B}{\tau - t^*}\right) \\ \quad \text{if } \tau \le t^* + \frac{x_L - x_B}{v_C} \\ N_B + (\tau - t^*) q_C - (x_L - x_B) k_C \\ \quad \text{if } \tau \ge t^* + \frac{x_L - x_B}{v_C} \end{cases}$	↤ min
[5] Piece of initial condition, type Free-flow, connected with piece of upstream boundary condition: 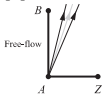	$\{x_0\} \times \{t^*\} \rightarrow$ $\{x_L\} \times \begin{bmatrix} t^* + \frac{L}{V(k_{A^+})}, \\ t^* + \frac{L}{V(q_{AZ})} \end{bmatrix}$	$N(x_L, \tau) = N_A - L\kappa\left(\frac{L}{\tau - t^*}\right)$	↤ min
[6] Piece of upstream boundary condition: 	$\{x_0\} \times [t_A, t_B] \rightarrow$ $\{x_L\} \times \begin{bmatrix} t_A + \frac{L}{V(q_{AB})}, \\ t_B + \frac{L}{V(q_{AB})} \end{bmatrix}$	$N(x_L, \tau) = \frac{(t_B - \tau)N_A + (\tau - t_A)N_B}{t_B - t_A} - LK\left(\frac{N_B - N_A}{t_B - t_A}\right)$	↤ min
[7] Consecutive pieces of upstream boundary condition: 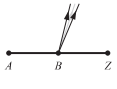	$\{x_0\} \times \{t_B\} \rightarrow$ $\{x_L\} \times \begin{bmatrix} t_B + \frac{L}{V(q_{AB})}, \\ t_B + \frac{L}{V(q_{BZ})} \end{bmatrix}$	$N(x_L, \tau) = N_B - L\kappa\left(\frac{L}{\tau - t_B}\right)$	↤ min

5. Simulation study

As a demonstration of the capabilities of the extended link model, we simulate the Dutch A13 motorway corridor from the Kleinpolderplein interchange near Rotterdam to the Ypenburg interchange near The Hague, with a length of 12 km, having five off-ramps and six on-ramps. Section 5.1 introduces the simulation setup and scenario, followed by visualisations of the results in Section 5.2 and model computation times in Section 5.3.

The raw input and output data of all simulations in this section are published by Van der Gun (2018).

Figure 10. A13 flow at crash location and applied traffic control.

5.1. Simulation setup and scenario

The link capacities in our simulations are based on the Dutch motorway capacity manual with a 2% truck percentage (Grontmij 2015), reduced with 5% to correct for the absence of a capacity drop in our current model. For uncontrolled links, we assume a free speed of 110 km/h, a critical speed of 90 km/h and a wave speed in congestion of -20 km/h. The node model is taken from Tampère et al. (2011). In the simulations, traffic is disaggregated using destination-based commodities (see Appendix 2).

The same corridor was already simulated in Van der Gun, Pel, and Van Arem (2017) for various evening peaks in September 2012. In this paper, we will focus on the evening peak of 11 September 2012. Around 15:45 that day, a crash occurred between the 10th off-ramp and on-ramp (University), just before the end of the peak hour lane. Despite the absence of injuries, the incident partly blocked the road for more than one hour until around 17:00, after which the released traffic triggers the recurrent bottleneck downstream of the 9th on-ramp (Delft). The flow and speed as measured on loop detectors just downstream of the incident location are shown in the top half of Figure 10.

During this evening peak, variable speed limits and dynamic lane management were applied, primarily through variable message signs (VMSs) mounted on gantries. The variable speed limits were partly set manually by the traffic management centre and partly automatically by the queue tail warning system (Dutch: filestaartbeveiliging). In both cases, the purpose is to avoid unsafe situations. The opening and closing of lanes are always manual. Besides lane closures at the incident location, the entire peak hour lane was closed for the duration of the incident, presumably to keep a clear path for emergency services. Within the simulated time period there were also two temporary closures of parts of the peak hour lane and the closure of the peak hour lane at the end of the peak period. All displayed

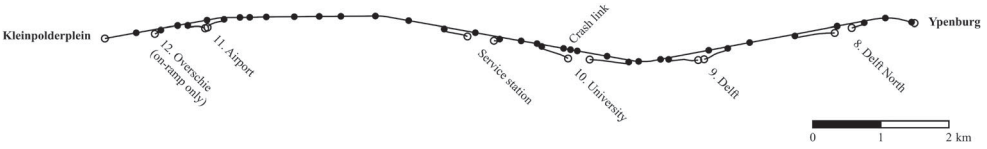

Figure 11. A13 corridor network.

speed limits and lane closures are visualised in the bottom half of Figure 10. They give rise to a substantial number of FD changes throughout the simulation, which makes this scenario an interesting test case for the link model improvements developed in this paper. In this demonstration, we will simply impose the speed limits as they were displayed in reality rather than making them responsive to the congestion as it occurs in the simulation, although we emphasise the latter is also possible with our model, since it does not need to know any FDs ahead of time.

To account for the spatial detail in the traffic control measures of this scenario – each link can only have one FD at a time – we split links at VMS gantries. For lane drops, the merging area is explicitly modelled with the capacity contribution of the terminating lane equal to 20% of a normal lane. We also insert an extra link of 100 m length around the crash location, so that we can separately model the driving behaviour near the crash location. The resulting network graph consists of 48 links and 49 nodes and is depicted in Figure 11.

For changes in the availability of lanes, we scale the FD of a link in the flow-density plane with respect to the origin towards the capacity value corresponding to the open lanes. We use the upstream gantry to decide whether lanes are open. The variable speed limits yield the following transformation of the FD in the speed-density plane:

$$\begin{pmatrix} k_C \\ k_J \\ u_F \\ u_C \end{pmatrix} \xrightarrow{VSL(\bar{u})} \begin{pmatrix} \max\left(k_C, \frac{k_J}{1-\bar{u}/v'}\right) \\ k_J \\ \bar{u} \\ \min(u_C, \bar{u}) \end{pmatrix}. \tag{16}$$

Similar to Hegyi, De Schutter, and Hellendoorn (2005a, 2005b), for each density, this transformation reduces the possible speeds to adhere to the new speed limit $\bar{u}$, while maintaining the extended Smulders FD shape. (Because the speed limits are not used for homogenisation purposes, a possible increase in capacity as suggested by, e.g. Cremer (1979) and Smulders (1990) is less important in this scenario.) To account for the relatively high non-compliance for VMS-displayed speed limits in the Netherlands, we add 20 km/h to the displayed speed limit in simulation. The speed limits are also taken from the upstream gantry, unless there is an on-ramp between the link and that gantry and the downstream gantry displays a higher speed limit.

During the incident, the crash link uses a triangular FD with a low capacity and a low free speed set based on measurements. The used parameters are indicated in the top half of Figure 10. Since the wave speed in congestion is unchanged, the jam density is also low. While the crash site could alternatively be modelled more simply as a single node with a node flow constraint, similar to e.g. the ramp metering by Hajiahmadi et al. (2013), we opted for a link to test our extended link model with relatively extreme FD changes.

Our simulation study also includes non-empty initial conditions at the start of the simulation for the motorway links. To construct the initial conditions, we take the first flow measurement from each loop detector, transform those into densities for each link using the free-flow FD branch and linearly interpolate the densities between the loops.

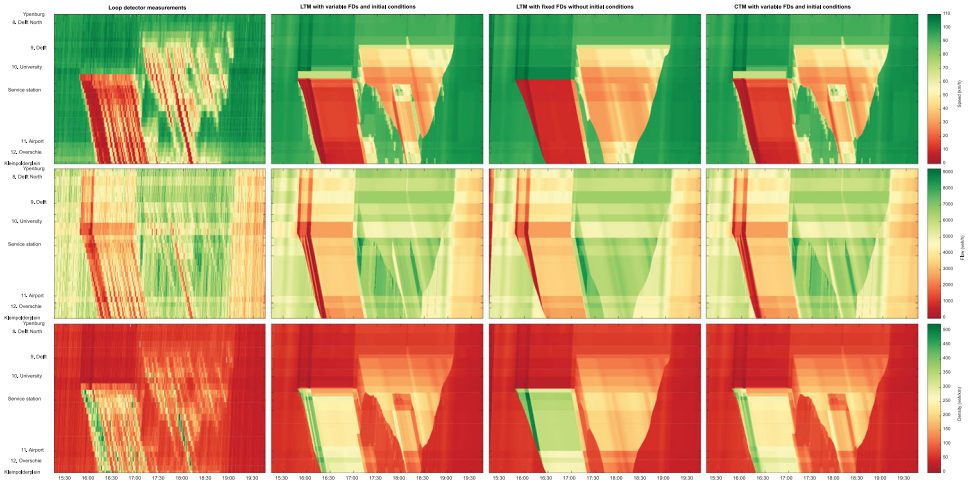

Figure 12. A13 measurements and simulation results for the extended LTM, traditional LTM, and extended CTM.

We conduct three separate simulations of this evening peak:

- The first simulation uses the LTM with variable FDs and initial conditions as proposed in this paper. Time step sizes differ per node based on the CFL conditions of connected links ($\Delta t \in \{1, \frac{1}{2}, \frac{1}{3}, \frac{1}{4}, \frac{1}{6}, \frac{1}{8}, \frac{1}{12}, \frac{1}{16}, \frac{1}{24}, \frac{1}{48}\}$ min).
- The second simulation uses the LTM with fixed FDs, i.e. no variable speed limits and an always-open peak hour lane, and without initial conditions. The capacity restriction at the crash site is modelled as a simple node flow constraint. Time step sizes again differ per node.
- The third simulation emulates the CTM solution scheme with variable FDs and initial conditions. It uses an equal time step size $\Delta t = \frac{1}{41}$ min for all nodes, based on the most constraining CFL condition. The number of cells is then maximised in each link, as this minimises the numerical error of the CTM (Van Wageningen-Kessels 2013). The CTM solution scheme is emulated by simplifying the initial conditions to a constant density per cell, updating these after every time step using CTM rules, and starting the next time step from the updated initial conditions.

5.2. Visualisations of simulation results

The simulation results are visualised in Figure 12, which shows the flow, speed and density from the loop detector measurements along with the results from the three simulations. Note that since Dutch loop detectors only record flow and time mean speed, the space mean speed is only an estimate and hence the density, computed as $k = q/u$, may be rather inaccurate for high densities (Knoop, Hoogendoorn, and Van Zuylen 2009). Because the LTM only computes traffic states at the boundaries of space–time rectangles as in Figure 3, the simulation results are further post-processed for the visualisation.

With the non-empty initial conditions, we see that the LTM no longer needs a warm-up period before providing realistic results. After the onset of the incident, the closing of the peak hour lane turns out to be important to reproduce the queue spillback – with fixed FDs, the queue density is too high and the spillback is too slow. The speed limits from the queue tail warning result in a more gradual speed reduction than just one shock, but, in accordance with Equation (16), do not affect traffic already driving slower than the new free speed.

The CTM and LTM with variable FDs and initial conditions yield very similar results, but the CTM has greater numerical diffusion. This increased diffusion in the CTM is particularly evident in the less crisp contact discontinuities between traffic states in congestion.

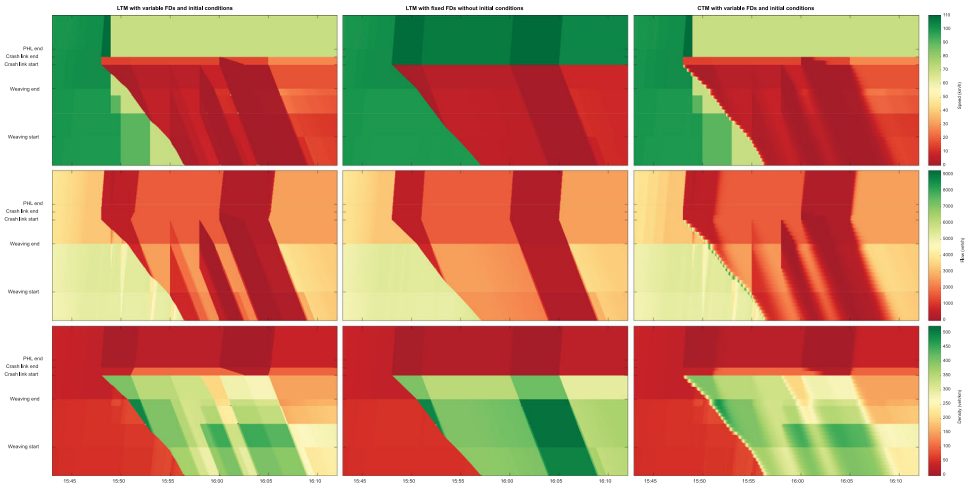

Figure 13. Congestion onset after the crash in simulation results for the extended LTM, traditional LTM, and extended CTM.

Figure 13 zooms in on the onset of congestion and shows that the extended LTM correctly handles FD changes that result in the jam density being exceeded. The solution contains two acceleration shocks, one on the crash link starting at 16:00 due to a change in driving behaviour at the crash location and one on the link before that starting at 15:58 due to a lane closure, and no negative flows or speeds occur. At this zoom level, we also clearly see that the numerical diffusion of the CTM is much greater than that of the LTM.

After the incident is cleared, the re-opening of the closed lanes and removal of the speed limits are well reproduced by the extended LTM link model. The growing oscillations in the congestion upstream of the incident and the stop-and-go waves originating from the recurrent bottleneck are not reproduced in the simulation, but these are well-known limitations of LWR theory to which the LTM and CTM calculate solutions. Despite this limitation, the shape of the congestion is reasonably well reproduced. One particularly interesting detail is that the most severe stop-and-go wave, reaching Kleinpolderplein around 18:10, does show up in the simulation – albeit with a lower density – due to an earlier lane drop making existing congestion more severe.

Overall, we conclude that our extended LTM works as expected based on LWR theory and our FD specifications, and that the simulation result indeed improves by taking the variable FDs and initial conditions into account. Compared to the CTM, this is achieved with considerably less numerical diffusion.

5.3. Model computation times

We finally compare the computation time of the simulations. In addition to the three simulations from the previous subsection, we include three more simulations where the LTMs and CTM use the same discretisation, i.e. an equal time step size $\Delta t = \frac{1}{41}$ min for all nodes and only one CTM cell per link. This decreases the accuracy and computation time for the CTM, but further increases the accuracy and computation time for the LTMs.

All six simulations of 4.5 hours simulated time are executed 101 times in randomised order, using a single thread on a PC with an Intel Xeon E5-1650 3.20 GHz CPU and 32 GB RAM. Table 5 lists the median execution times per simulation type. The execution times include initialisation of the simulation model but exclude file input/output. The post-processing of results for visualisations like in the previous subsection is also excluded from this benchmark.

The results show that the (extended) LTM can be a very fast simulation tool. Despite the large number of FD changes in our simulated scenario, we see that their impact on the computation time of

Table 5. Computation times of the simulations.

	LTM with variable FDs and initial conditions	LTM with fixed FDs without initial conditions	CTM with variable FDs and initial conditions
Optimal discretisation (Section 5.2)	0.073 s	0.064 s	0.296 s
Equal discretisation (equal time steps, one CTM cell per link)	0.239 s	0.228 s	0.271 s

the LTM remains fairly small. The ability of the LTM to use different time step sizes per node greatly improves its performance in a network with some short links, while remaining very accurate. Our extended LTM is about four times as fast as a CTM for a comparable numerical accuracy as in Figure 12. Conversely, with an equal discretisation and similar computation time, our extended LTM has considerably better numerical accuracy than the CTM. Despite being important for CTM accuracy, the number of cells within links only has a minor impact on CTM efficiency because their computations are a lot simpler than general nodes.

6. Discussion

In our link model formulation, all vehicles simultaneously on a link are assumed to adhere to the same FD, and thus simultaneously change their driving behaviour when a new FD is specified for the link. Some researchers might instead prefer a model that uses a multi-class LWR theory (Logghe and Immers 2008), which was applied by Smits, Bliemer, and Van Arem (2011) and Hajiahmadi et al. (2013) in an LTM context. Such multi-class approaches allow e.g. assigning driving behaviour to vehicles upon the moment they enter the link, which they then retain while driving on the link, which Hajiahmadi et al. (2013) did for variable speed limits. This may be more realistic in some cases, e.g. when traffic rules for the link are displayed on gantries at the link entrance like in our case study, as drivers are unable to see rule changes after they entered the link. However, there are also important disadvantages to this alternative modelling approach. Firstly, it becomes much more difficult to develop a non-cell-based solution scheme, particularly when the model simultaneously has to support non-triangular FDs whose parameters can vary arbitrarily, and first-in-first-out behaviour no longer applies. Secondly, the assumption of driving behaviour being fixed after entering the link may itself be invalid, as drivers notice other drivers behaving differently, if drivers adapt to VMSs they see downstream, if information is provided in-vehicle, or if the FD change reflects a change in environmental conditions such as the weather.

For readers primarily interested in using our model to start their simulations with a non-empty network, we would like to remark that this uses as input an explicit initial distribution of density over space, and that this is not the only possible way to start an LTM simulation with a non-empty network. For example, when simulating two scenarios that only diverge after a certain point in time, it can be more convenient to simply make a copy of the model's computer memory at that point in simulation time, than to compute the within-link densities and use those to start the second simulation. Similarly, in our case study we could alternatively have used loop flow measurements from shortly before the studied time period to warm up the links. This however does rely on the initial data indeed consisting of point measurements over some prior time period (as opposed to spatial measurements at one moment in time) during which the FD is known, and if the FD changes during or prior to the simulation, one still needs to use our extended link model.

Another point of discussion is the chosen Smulders FD shape. While the choice of this specific shape is a limitation compared to other LTM formulations supporting more general FD shapes, our chosen free-flow branch shape does support subcritical delays and platoon dispersion. Although the shape of the congested branch is less sophisticated, we believe it suffices for most use cases, and its simplicity allows us to compute within-link densities without having to wait for all slow congested waves from the initial condition to leave the link. The non-negativity of speeds and flows when densities exceed the jam density enhances the robustness of model applications.

One previous LTM feature that is nevertheless missing from our current FD shape is a capacity drop. Van der Gun, Pel, and Van Arem (2017) previously formulated such an extension to the LTM, using an inverted-lambda style FD, which was able to produce stop-and-go waves. As a generalisation of Algorithm 6 in their paper, it is possible to divide the within-link space into an area where only free-flow traffic states and one selected 'coasting state' with a density higher than the free-flow critical density, and a more downstream area where only traffic states with flows lower than the queue discharge rate can occur. This can be used to algebraically compute within-link densities, also in case of an initial condition. However, we are not aware of whether/how one can simultaneously satisfy Equation (7). The adaptation to include a capacity drop also makes the derivation and formulation of the extended LTM considerably different, more complex, and harder to understand from the perspective of traditional LWR theory. For these reasons, we chose to not include a capacity drop in this paper. We do encourage future research into this topic because depending on its results, it could be very useful to combine a capacity drop and support for link-based traffic management in one simulation model.

As an alternative to our chosen Smulders FD in the current paper, we could have adopted an FD that is piecewise-linear in the flow-density plane in its entirety. Since this results in less smooth subcritical delay function than Figure 1, we believe this can only be beneficial if combined with an event-based continuous-time network solution scheme (Raadsen and Bliemer 2018) instead of the less-complex and more-developed discrete-time scheme we used. An event-based adaptation of our work can however be an interesting avenue for future research that is likely feasible.

Some readers may wonder whether our extended link model can be embedded in the iterative LTM solution scheme (Himpe, Corthout, and Tampère 2016), allowing larger time steps than Equation (2) and warm-starting an optimisation or equilibration procedure (Himpe and Tampère 2016). In this case, the most recent parts of the link boundary conditions that are needed for the computation of sending and receiving flows, are not yet known, but an estimate is available, allowing those estimates to be iteratively updated until sufficient convergence is reached. Hence, it is possible to make it work. First, at the start of a time step, one takes the discrete-time constraints on future cumulative inflows and outflows and makes a back-up copy in computer memory. Then, 'update' the link boundary conditions as estimated, and compute the sending and receiving flows. As long as another iteration of the same time step is necessary, revert the constraints to their back-up copy and 'update' them with the newer estimates instead. Once converged, continue with the next time step. Because the support for initial conditions in the sending and receiving flow computations is retained and the computation of within-link densities is not affected by the larger time steps, this makes all features of our extended link model available.

Finally, we emphasise the computational efficiency of our extended link model. Based on our remarks in Section 4.4 and Appendix A.2, we conclude that the computation of sending and receiving flows requires the same or fewer iterations than previous discrete-time link model formulations in literature. Each computation of within-link density profiles and application of initial conditions only incurs a one-time computational cost per link, so the additional computation time for these new features should be limited for most applications, e.g. in case of a limited number of FD changes. The high numerical accuracy of the LTM is preserved. The high efficiency and accuracy have been validated in Section 5.

The computer memory requirements are also limited and independent of the duration of the simulation. For the calculation of within-link densities, only the most recent parts of the downstream boundary condition (last $-L/v'$ time) and the upstream boundary condition (last L/v_C time) need to be known. Older traffic states from the boundary conditions cannot affect the current within-link densities anymore and can thus be forgotten, so that longer simulations do not require more computer memory. Note that the initial condition must be remembered, since initial densities exceeding the jam density may remain present on the link indefinitely. The computations of the receiving and sending flows additionally need to store cumulative inflow and outflow constraints for a finite number of time points in the near future. These data can be handled efficiently using a (variable-size) circular buffer data structure instead of a traditional array.

7. Conclusions

With a derivation from LWR theory, we extended the link model of the discrete-time LTM with the capabilities of using non-empty initial conditions and computing within-link density profiles, using a Smulders FD with no negative flows or speeds beyond the jam density. When combined, they can be used to fuse data or to instantaneously change the FDs of links within an LTM simulation. These extra capabilities, which were previously only available using memory-less numerical schemes like the CTM, introduce no new numerical error to the LTM. Since each invocation of the new capabilities involves only a one-time computational cost penalty, the LTM remains suitable for the efficient multi-commodity simulation of large general networks, and outperforms the CTM.

We demonstrated the benefit of the abilities to change FDs and use initial conditions with a numerical example with variable speed limits and dynamic lane management. These and other possible applications of this robust general-purpose link model extension, e.g. involving traffic control, changes in environmental conditions and driver behaviour, and real-time forecasts significantly extend the potential application domain of the LTM and, by extension, efficient large-scale simulations based on LWR theory. We look forward to future research on such advanced applications.

Disclosure statement

No potential conflict of interest was reported by the authors.

Funding

This research effort is funded by the NWO-NSFC (Netherlands Organisation for Scientific Research, National Natural Science Foundation of China) project 'Optimal Multimodal Network Management for Urban Emergencies', part of the China–Netherlands joint research program 'The Application of Operations Research in Urban Transport'.

ORCID

Jeroen P. T. van der Gun http://orcid.org/0000-0002-6522-3657
Adam J. Pel http://orcid.org/0000-0003-3754-5779
Bart van Arem http://orcid.org/0000-0001-8316-7794

References

Bliemer, M. C. J., and M. P. H. Raadsen. 2018. "Continuous-time General Link Transmission Model with Simplified Fanning, Part I: Theory and Link Model Formulation." *Transportation Research Part B*. doi:10.1016/j.trb.2018.01.001.

Chung, E., O. Ohtani, H. Warita, M. Kuwahara, and H. Morita. 2006. "Does Weather Affect Highway Capacity?" Proceedings of the 5th International Symposium on Highway Capacity and Quality of Service, Yokohama, Japan, 139–146.

Courant, R., K. Friedrichs, and H. Lewy. 1928. "Über die Partiellen Differenzengleichungen der Mathematischen Physik." *Mathematische Annalen* 100: 32–74.

Cremer, M. 1979. *Der Verkehrsfluß auf Schnellstraßen: Modelle, Überwachung, Regelung*. Berlin: Springer-Verlag.

Daganzo, C. F. 1994. "The Cell Transmission Model: A Dynamic Representation of Highway Traffic Consistent with the Hydrodynamic Theory." *Transportation Research Part B* 28 (4): 269–287.

Daganzo, C. F. 1995. "The Cell Transmission Model, Part II: Network Traffic." *Transportation Research Part B* 29 (2): 79–93.

Daganzo, C. F. 2005. "A Variational Formulation of Kinematic Waves: Basic Theory and Complex Boundary Conditions." *Transportation Research Part B* 39 (2): 187–196.

Dixit, V. V., V. V. Gayah, and E. Radwan. 2012. "Comparison of Driver Behavior by Time of Day and Wet Pavement Conditions." *Journal of Transportation Engineering* 138 (8): 1023–1029.

Evans, L. C. 2002. "Nonlinear First-Order PDE." In *Partial Differential Equations*, 94–174. Providence, Rhode Island: American Mathematical Society.

Geistefeldt, J. 2012. "Operational Experience with Temporary Hard Shoulder Running in Germany." *Transportation Research Record* 2278: 67–73.

Gentile, G. 2010. "The General Link Transmission Model for Dynamic Network Loading and a Comparison with the DUE Algorithm." In *New Developments in Transport Planning: Advances in Dynamic Traffic Assignment*, edited by C. M. J. Tampère, F. Viti, and L. H. Immers, 153–178. Cheltenham: Edward Elgar.

Gentile, G. 2015. "Using the General Link Transmission Model in a Dynamic Traffic Assignment to Simulate Congestion on Urban Networks." *Transportation Research Procedia* 5: 66–81.

Gentile, G., L. Meschini, and N. Papola. 2007. "Spillback Congestion in Dynamic Traffic Assignment: A Macroscopic Flow Model with Time-Varying Bottlenecks." *Transportation Research Part B* 41 (10): 1114–1138.

Gentile, G., and N. Papola. 2009a. "Dynamic Traffic Assignment with Nonseparable Link Cost Functions and Queue Spillovers." In *Transportation Systems Analysis: Models and Applications*, edited by E. Cascetta, 464–480. New York: Springer.

Gentile, G., and N. Papola. 2009b. "The Simplified Theory of Kinematic Waves Based on Cumulative Flows: Application to Macroscopic Link Performance Models." In *Transportation Systems Analysis: Models and Applications*, edited by E. Cascetta, 497–510. New York: Springer.

Geroliminis, N., and A. Skabardonis. 2005. "Prediction of Arrival Profiles and Queue Lengths Along Signalized Arterials by Using a Markov Decision Process." *Transportation Research Record* 1934: 116–124.

Grontmij. 2015. *Capaciteitswaarden Infrastructuur Autosnelwegen*. 4th ed. The Hague: Dienst Water, Verkeer en Leefomgeving.

Guerrieri, M., and R. Mauro. 2016. "Capacity and Safety Analysis of Hard-Shoulder Running (HSR). A Motorway Case Study." *Transportation Research Part A* 92: 162–183.

Hajiahmadi, M., R. Corthout, C. Tampère, B. De Schutter, and H. Hellendoorn. 2013. "Variable Speed Limit Control Based on Extended Link Transmission Model." *Transportation Research Record* 2390: 11–19.

Hajiahmadi, M., G. S. van de Weg, C. M. J. Tampère, R. Corthout, A. Hegyi, B. De Schutter, and H. Hellendoorn. 2016. "Integrated Predictive Control of Freeway Networks Using the Extended Link Transmission Model." *IEEE Transactions on Intelligent Transportation Systems* 17 (1): 65–78.

Han, K., T. L. Friesz, W. Y. Szeto, and H. Liu. 2015. "Elastic Demand Dynamic Network User Equilibrium: Formulation, Existence and Computation." *Transportation Research Part B* 81: 183–209.

Han, K., B. Piccoli, and W. Y. Szeto. 2016. "Continuous-time Link-Based Kinematic Wave Model: Formulation, Solution Existence, and Well-Posedness." *Transportmetrica B* 4 (3): 187–222.

Hegyi, A., B. De Schutter, and J. Hellendoorn. 2005a. "Optimal Coordination of Variable Speed Limits to Suppress Shock Waves." *IEEE Transactions on Intelligent Transportation Systems* 6 (1): 102–112.

Hegyi, A., B. De Schutter, and J. Hellendoorn. 2005b. "Model Predictive Control for Optimal Coordination of Ramp Metering and Variable Speed Limits." *Transportation Research Part C* 13 (3): 185–209.

Himpe, W., R. Corthout, and C. M. J. Tampère. 2016. "An Efficient Iterative Link Transmission Model." *Transportation Research Part B* 92 (B): 170–190.

Himpe, W., and C. M. J. Tampère. 2016. "A Dynamic User Equilibrium Algorithm that Exploits Warm Starting Capabilities of the Iterative Link Transmission Model." International Symposium on Dynamic Traffic Assignment, Sydney, Australia.

Jin, W. 2015. "Continuous Formulations and Analytical Properties of the Link Transmission Model." *Transportation Research Part B* 74: 88–103.

Knoop, V. L., S. P. Hoogendoorn, and H. J. Van Zuylen. 2009. "Empirical Differences Between Time Mean Speed and Space Mean Speed." In *Traffic and Granular Flow '07*, edited by C. Appert-Rolland, F. Chevoir, P. Gondret, S. Lassarre, J. P. Lebacque, and M. Schreckenberg, 351–356. Berlin: Springer-Verlag.

Kwon, T. J., L. Fu, and C. Jiang. 2013. "Effect of Winter Weather and Road Surface Conditions on Macroscopic Traffic Parameters." *Transportation Research Record* 2329: 54–62.

Lax, P. D. 1957. "Hyperbolic Systems of Conservation Laws II." *Communications on Pure and Applied Mathematics* 10 (4): 537–566.

Lebacque, J., and M. Khoshyaran. 2005. "First-Order Macroscopic Traffic Flow Models: Intersection Modeling, Network Modeling." In *Transportation and Traffic Theory: Flow, Dynamics and Human Interaction*, edited by H. S. Mahmassani, 365–386. Amsterdam: Elsevier.

Lighthill, M. J., and G. B. Whitham. 1955. "On Kinematic Waves II. A Theory of Traffic Flow on Long Crowded Roads." *Proceedings of the Royal Society of London A* 229 (1178): 317–345.

Logghe, S., and L. H. Immers. 2008. "Multi-class Kinematic Wave Theory of Traffic Flow." *Transportation Research Part B* 42: 523–541.

Long, J., J. Chen, W. Y. Szeto, and Q. Shi. 2018. "Link-based System Optimum Dynamic Traffic Assignment Problems with Environmental Objectives." *Transportation Research Part D* 60: 56–75.

Long, Jiancheng, W. Y. Szeto, and Jianxun Ding. 2017. "Dynamic Traffic Assignment in Degradable Networks: Paradoxes and Formulations with Stochastic Link Transmission Model." *Transportmetrica B: Transport Dynamics*: 1–27. doi:10.1080/21680566.2017.1405749.

Luke, J. C. 1972. "Mathematical Models for Landform Evolution." *Journal of Geophysical Research* 77 (14): 2460–2464.

Newell, G. F. 1993. "A Simplified Theory of Kinematic Waves in Highway Traffic, Part I: General Theory." *Transportation Research Part B* 27 (4): 281–287.

Papageorgiou, M., C. Diakaki, V. Dinopoulou, A. Kotsialos, and Y. Wang. 2003. "Review of Road Traffic Control Strategies." *Proceedings of the IEEE* 91 (12): 2043–2067.

Raadsen, M. P. H., and M. C. J. Bliemer. 2018. "Continuous-time General Link Transmission Model with Simplified Fanning, Part II: Event-based Algorithm for Networks." *Transportation Research Part B*. doi:10.1016/j.trb.2018.01.003.

Raadsen, M. P. H., M. C. J. Bliemer, and M. G. H. Bell. 2016a. "An Efficient and Exact Event-based Algorithm for Solving Simplified First Order Dynamic Network Loading Problems in Continuous Time." *Transportation Research Part B* 92 (B): 191–210.
Rakha, H., M. Farzaneh, M. Arafeh, and E. Sterzin. 2008. "Inclement Weather Impacts on Freeway Traffic Stream Behavior." 87th Transportation Research Board Annual Meeting, Washington, DC.
Richards, P. I. 1956. "Shock Waves on the Highway." *Operations Research* 4 (1): 42–51.
Smits, E., M. C. J. Bliemer, A. J. Pel, and B. Van Arem. 2015. "A Family of Macroscopic Node Models." *Transportation Researsch Part B* 74: 20–39.
Smits, E., M. C. J. Bliemer, and B. Van Arem. 2011. "Dynamic Network Loading of Multiple User-Classes with the Link Transmission Model." 2nd International Conference on Models and Technologies for Intelligent Transportation Systems, Leuven, Belgium.
Smulders, S. 1990. "Control of Freeway Traffic Flow by Variable Speed Signs." *Transportation Research Part B* 24B (2): 111–132.
Sultan, B., R. Meekums, and M. Brown. 2008. "The Impact of Active Traffic Management on Motorway Operation." IET Road Transport Information and Control Conference and ITS United Kingdom Members' Conference. Manchester, 180–187.
Tampère, C. M. J., R. Corthout, D. Cattrysse, and L. H. Immers. 2011. "A Generic Class of First Order Node Models for Dynamic Macroscopic Simulation of Traffic Flows." *Transportation Research Part B* 45 (1): 289–309.
Van der Gun, J. P. T. 2018. "A13 Motorway Simulation Study Data for the Link Transmission Model with Variable Fundamental Diagrams and Initial Conditions." *4TU.ResearchData*. doi:10.4121/uuid:c7dd3a61-1bed-4858-b294-93acd960a645.
Van der Gun, J. P. T., A. J. Pel, and B. Van Arem. 2016. "Propagating Agents with Macroscopic Dynamic Network Loading: Challenges and Possible Solutions." *Procedia Computer Science* 83: 914–920.
Van der Gun, J. P. T., A. J. Pel, and B. Van Arem. 2017. "Extending the Link Transmission Model with non-Triangular Fundamental Diagrams and Capacity Drops." *Transportation Research Part B* 98: 154–178.
Van de Weg, G. S., M. Keyvan-Ekbatani, A. Hegyi, and S. P. Hoogendoorn. 2016. "Urban Network Throughput Optimization via Model Predictive Control Using the Link Transmission Model." Transportation Research Board Annual Meeting, Washington, DC.
Van Wageningen-Kessels, F. L. M. 2013. "Numerical Methods for Mixed-class Models." Chap. 8 in *Multi-class Continuum Traffic Flow Models: Analysis and Simulation Methods*, PhD diss., Delft University of Technology, 159–189.
Wolshon, B., and L. Lambert. 2006. "Reversible Lane Systems: Synthesis of Practice." *Journal of Transportation Engineering* 132 (12): 933–944.
Yperman, I. S. 2007. "The Link Transmission Model for Dynamic Network Loading." PhD diss., KU Leuven.
Yperman, I. S., S. Logghe, and L. H. Immers. 2005. "The Link Transmission Model: An Efficient Implementation of the Kinematic Wave Theory in Traffic Networks." 10th EURO Working Group on Transportation Meeting, Poznan, Poland, 122–127.
Yperman, I. S., S. Logghe, C. M. J. Tampère, and L. H. Immers. 2006. "The Multi-Commodity Link Transmission Model for Dynamic Network Loading." 85th Transportation Research Board Annual Meeting, Washington, DC.
Yuan, Y., A. J. Pel, and S. P. Hoogendoorn. 2014. "The Transition Between Normal and Emergency Driving Behaviour During Evacuation And Its Implications For Traffic Flow Operations and Traffic Management." 17th IEEE International Conference on Intelligent Transportation Systems, Qingdao, China, 2700–2705.

Appendices

Appendix 1: Notation

Coordinates	
x	location
x_0	location of upstream link end
x_L	location of downstream link end
L	link length
t	time in general or current time
τ	time in general
t^*	time of most recent initial condition
Δt	time step size
Δt_{x_0}	time step size of upstream node
Δt_{x_L}	time step size of downstream node
Link transmission model structure	
$S(t), \quad S_i(t)$	sending flow (of link i) in time step starting at time t
$S_{ij}(t)$	part of sending flow of link i destined for link j in time step starting at time t

$R(t)$, $R_j(t)$	receiving flow (of link j) in time step starting at time t
$G_{ij}(t)$	transition flow from link i to link j in time step starting at time t
Traffic flow theory	
k, $k(x,t)$	density (at space–time point (x,t))
q, $q(x,t)$	flow (at space–time point (x,t))
N, $N(x,t)$	cumulative number of vehicles (at space–time point (x,t))
$N^{\max}(x,t)$	upper bound on cumulative number of vehicles at space–time point (x,t)
Fundamental diagram	
$Q(k)$	flow as function of density k
$U(k)$	speed as function of density k
$V(k)$, $V(q)$	free-flow branch wave speed as function of density k or flow q
$K(q)$	free-flow branch density as function of flow q
$\kappa(v)$	flow-density plane tangent line density-axis intercept (non-positive) as function of free-flow branch wave speed v
u_F	free speed
u_C	critical speed, i.e. speed at capacity
k_C	critical density, i.e. density at capacity
v_C	critical wave speed, i.e. maximum wave speed at capacity
v'	wave speed in congestion (negative)
k_J	jam density
Piecewise descriptions	
x_A	location of point A
t_A	time of point A
N_A	cumulative number of vehicles of point A
f_{AB}	second spatial derivative of cumulative number of vehicles on piece AB
$N_{AB}(x)$, $N_{AB}(\tau)$	cumulative number of vehicles on piece AB as function of location x or time τ
q_{AB}	flow on piece AB
k_{A+}	density immediately downstream of point A
k_{A-}	density immediately upstream of point A

Appendix 2: Multi-commodity support

Since Yperman et al. (2006), the LTM can be used in a multi-commodity fashion, e.g. to disaggregate traffic by destination for route choice purposes. Yperman et al. (2006) disaggregate traffic (potentially) leaving a link by looking at the traffic composition when this traffic entered the link. We note that this is problematic when the network is not empty at the start of the simulation. There are two possible solutions.

The first solution is to construct a virtual link inflow history prior to the start of the simulation, which is then only used to disaggregate traffic on the link. This is the solution we use for the simulations in Section 5. Multiple virtual past time steps can be used to denote changes in initial traffic composition along the link.

Alternatively, this problem can be avoided by instead storing the traffic composition per link as an explicit first-in-first-out (FIFO) queue in computer memory, whose initial state can be provided along with the initial conditions for the traffic positioning on the link. Here, 'queue' refers to the computer data structure, not to the traffic phenomenon. Each entry in this queue is an unordered collection of pairs of vehicle type and vehicle amount. Each time step, each node partially or completely consumes entries from the fronts of the queues of incoming links until it cannot accept more flow, and adds a new entry to the backs of the queues of each outgoing link that receives flow. For partially consumed entries, the consumption of vehicle types is proportional to their amounts.

A secondary benefit of such an explicit FIFO queue is that it is more efficient, since the computational cost of disaggregation no longer depends on the total number of commodities in the link or network, and it avoids storing a separate cumulative inflow history per commodity in memory. The node model algorithm can be modified to prefer strict FIFO over strict conservation of turning fractions. (Node model applications usually prefer strict conservation of the specified turning fractions, that is, when they change the outflow of a link, the composition of this outflow is not updated accordingly.) We refer to Van der Gun, Pel, and Van Arem (2016, 918) for a further elaboration.

Appendix 3: Conflict resolution examples

In this appendix, we explain the conflict resolution for Section 4 in more detail, with two examples: computing the within-link density profile in continuous coordinates (Part A.1) and computing link outflow constraints in discrete coordinates (Part A.2).

A.1. Conflict resolution in continuous coordinates

Suppose we are calculating the within-link density profile, for which the intermediate solution so far consists of four pieces *EF*, *FG*, *GH*, and *HI* ($x_E < x_F < x_G < x_H < x_I, N_E \geq N_F \geq N_G \geq N_H \geq N_I$). Using the second and third columns of Table 2, we construct some new candidate piece *OP* ($x_O < x_P, N_O \geq N_P$). Suppose the conflict resolution method indicated in the fourth column is '$\overset{\uparrow}{\uparrow}$ min'. The upward '$\overset{\uparrow}{\uparrow}$ ' arrow means we start at low x, i.e. we first decide whether the upstream point *O* of the candidate piece should be added to the intermediate solution. This is the case if x_O lies in front of the previous upstream end of the intermediate solution ($x_O < x_E$) or if N_E is smaller (because of 'min') than the previous intermediate solution evaluated at x_0.

If true, and if $x_P > x_E$, we need to find the shock between the new candidate characteristics and those of the previous intermediate solution. In this example we assume $x_F \leq x_O < x_G$. Then, piece *EF* can be discarded immediately since only the new candidate piece can be upstream of the shock (because of '$\overset{\uparrow}{\uparrow}$ '). The next piece of the previous intermediate solution is *FG*. If $x_G \leq x_P$ and $N_{OP}(x_G)$, the cumulative value of piece *OP* evaluated at x_G, is smaller (because of 'min') than N_G, piece *FG* is also discarded. This is repeated until a next piece, e.g. piece *HI*, for which this condition no longer holds. Finally, solving

$$\begin{cases} N_{OP}(x) - N_{HI}(x) = 0 \\ \dfrac{\mathrm{d}}{\mathrm{d}x}(N_{OP}(x) - N_{HI}(x)) > 0 \end{cases} \tag{A1}$$

for x using the quadratic formula ($>$ because 'min') gives the location of the shock, to which both pieces are then truncated. The new candidate piece is now added to the intermediate solution.

Implementers are advised to be wary of the finite precision of floating-point number representations, to prevent rounding errors from resulting in extremely short pieces in the calculated solution that do not exist in the true algebraic solution.

A.2. Conflict resolution in discrete coordinates

Suppose we are calculating the link cumulative outflow constraints with discrete time steps, for which the intermediate solution so far is

$$\begin{cases} N^{\max}(x_L, t + \Delta t_{x_L}) = N_1 \\ N^{\max}(x_L, t + 2\Delta t_{x_L}) = N_2 \\ N^{\max}(x_L, t + 3\Delta t_{x_L}) = N_3 \\ N^{\max}(x_L, t + 4\Delta t_{x_L}) = N_4 \\ N^{\max}(x_L, t + n\Delta t_{x_L}) = N_5 + (n-5)q_C\Delta t_{x_L} \forall n \in \{5, 6, 7, \ldots\} \end{cases} \tag{A2}$$

for some N_1, N_2, N_3, N_4, N_5. Using the second and third columns of Table 4, we construct some new constraints

$$\begin{cases} \hat{N}^{\max}(x_L, t + 2\Delta t_{x_L}) = \hat{N}_2 \\ \hat{N}^{\max}(x_L, t + 3\Delta t_{x_L}) = \hat{N}_3 \\ \hat{N}^{\max}(x_L, t + 4\Delta t_{x_L}) = \hat{N}_4 \\ \hat{N}^{\max}(x_L, t + 5\Delta t_{x_L}) = \hat{N}_5 \end{cases} \tag{A3}$$

with some $\hat{N}_2, \hat{N}_3, \hat{N}_4, \hat{N}_5$. The conflict resolution method indicated in the fourth column is '↞ min'. The leftward '↞ ' arrow means we start at a high time, i.e. we first decide whether the constraint at time $t + 5\Delta t_{x_L}$ must be lowered in our intermediate solution (because of 'min').

If true ($\hat{N}_5 < N_5$), we need to find the shock between the new candidate characteristics and those of the previous intermediate solution. We update the intermediate solution at $t + 5\Delta t_{x_L}$, and discard the previous constraints for time $t + 6\Delta t_{x_L}$ and later since the shock must be before the new candidate characteristics (because of '↞ '). We next look at time $t + 4\Delta t_{x_L}$ and update it as well if $\hat{N}_4 < N_4$. This iteration continues until all new constraints are processed or until e.g. $t + 3\Delta t_{x_L}$ if $\hat{N}_3 \geq N_3$. The updated intermediate solution is now

$$\begin{cases} N^{\max}(x_L, t + \Delta t_{x_L}) = N_1 \\ N^{\max}(x_L, t + 2\Delta t_{x_L}) = N_2 \\ N^{\max}(x_L, t + 3\Delta t_{x_L}) = N_3 \\ N^{\max}(x_L, t + 4\Delta t_{x_L}) = \hat{N}_4 \\ N^{\max}(x_L, t + 5\Delta t_{x_L}) = \hat{N}_5 \end{cases} \tag{A4}$$

Note that this searching direction allows terminating the iteration as soon as the shock is found; e.g. the computation of $\hat{N}_2$ can be skipped. This avoids the need to iterate over the entire new set of candidate characteristics when not all of them are relevant, increasing computational efficiency compared to Gentile and Papola (2009b) and Gentile (2010).